Geological Society of America Special Papers

Controls on the erosion and geomorphic evolution of the San Bernardino and San Gabriel Mountains, southern California

James A. Spotila, Martha A. House, Ann E. Blythe, Nathan A. Niemi and Gregory C. Bank

Geological Society of America Special Papers 2002;365;205-230
doi: 10.1130/0-8137-2365-5.205

Geological Society of America
Special Paper 365
2002

Controls on the erosion and geomorphic evolution of the San Bernardino and San Gabriel Mountains, southern California

James A. Spotila
Department of Geological Sciences, 4044 Derring Hall, Virginia Polytechnic Institute and State University, Blacksburg, Virginia 24061, USA
Martha A. House
Geological and Planetary Sciences, MS100-23, California Institute of Technology, Pasadena, California 91125, USA
Ann E. Blythe
Department of Earth Sciences, University of Southern California, Los Angeles, California 90089, USA
Nathan A. Niemi*
California Institute of Technology Pasadena, California 91125, USA
Gregory C. Bank*
Virginia Polytechnic Institute and State University, Blacksburg, Virginia 24061, USA

ABSTRACT

We have investigated what controls geomorphic evolution of active mountain belts by comparing the patterns of erosion in the San Gabriel and San Bernardino Mountains of southern California. These siblings in the Central Transverse Ranges are juxtaposed across the San Andreas fault and have been tectonically uplifted since the late Miocene under roughly similar conditions, yet their geomorphic expressions are very different. Because these ranges share numerous boundary conditions and because their syn-uplift exhumation is constrained by thermochronometric and geologic data, they provide a template to explore the role of specific parameters on the erosion of mountains. To address this, existing constraints on long-term exhumation are synthesized and used to construct best-guess models of erosion patterns in each range. These patterns of erosion are then compared to variables that are generally considered to be important influences on erosion rate. Erosion rate is correlated with topographic slope, suggesting that the two are coupled and that the questions of what controls erosion and what controls topography are interchangeable. Erosion patterns are also strongly influenced by the distribution of active structures, suggesting that deformation alone may be responsible for the observed patterns within each range. However, additional correlations with erosion exist in bedrock erodibility and mean annual precipitation. Altogether, broad differences between the two ranges may be explained by either structure, bedrock erodibility, long-term precipitation, or the greater duration of uplift of the San Gabriel Mountains. All of the boundary conditions that are generally considered important in the erosion of mountains are thus found to be related to erosion patterns in the Central Transverse Ranges. Without a means to

*Present addresses: Niemi—Department of Earth, Atmospheric, and Planetary Sciences, Massachusetts Institute of Technology, 77 Massachusetts Avenue, Cambridge, Massachusetts 02139, USA; Bank—Advanced Resources International, Inc., 1110 North Glebe Road, Suite 600, Arlington, Virginia, 22201, USA.

Spotila, J.A., House, M.A., Blythe, A.E., Niemi, N.A., and Bank, G.C., 2002, Controls on the erosion and geomorphic evolution of the San Bernardino and San Gabriel Mountains, southern California, *in* Barth, A., ed., Contributions to Crustal Evolution of the Southwestern United States: Boulder, Colorado, Geological Society of America Special Paper 365, p. 205–230.

isolate the relative influence of each parameters, however, we conclude that geomorphic differences between the ranges are the result of coincidental spatial arrangement of independent variables that are important for sculpting mountains.

INTRODUCTION

At first glance, the San Gabriel and San Bernardino Mountains of southern California may appear as mirror images of each other. Both crystalline masses sit astride the San Andreas fault and display the anomalous east-west fabric of the Transverse Ranges, in contrast to the northwest-trending structural grain typical of the Pacific-North American plate boundary (Fig. 1) (Baird et al., 1974). Both have risen in association with transpression since opening of the Gulf of California in the late Miocene (Atwater, 1970; Weldon et al., 1993; Dickinson, 1996; Ingersoll and Rumelhart, 1999; Nagy and Stock, 2000). Both have been uplifted primarily on reverse fault systems that dip toward the San Andreas fault, mimicking a classic transpressional flower structure (e.g., Sylvester, 1988; Vauchez and Nicolas, 1991). The two ranges are also nearly identical in map-view dimensions, relief, and peak height.

Despite these similarities, these ranges are fundamentally different in many respects. The crystalline basement of each range is distinct both petrologically and in long-term deformation history (Morton, 1975; Ehlig, 1981; Dibblee, 1982a, 1982b; Powell, 1982; Morton and Matti, 1993). Each broadly consists of granitic plutons of the Mesozoic volcanic arc, sedimentary remnants of the Paleozoic miogeocline, and Precambrian gneiss assemblages (Dibblee, 1982a, 1982b; Morton and Matti, 1993; Barth et al., 1995), but the lithologic assemblages are distinct and originated >300 km apart prior to dextral translation along the San Andreas fault system since the early Miocene (Weldon et al., 1993; Powell, 1993; Dillon and Ehlig, 1993). The transpressive deformation and uplift history of these ranges are also distinct. The San Bernardino Mountains have risen rapidly within the past 2–3 m.y., based on numerous stratigraphic and thermochronometric constraints (Dibblee, 1975; May and Repenning, 1982; Sadler, 1982; Meisling and Weldon, 1989; Spotila et al., 1998; Albright, 1999; Spotila et al., 2001). In contrast, the San Gabriel Mountains have experienced rapid transpressive uplift for the past 5–7 m.y. (Crowell, 1982; Dibblee, 1982a; Wright, 1991; Bull, 1991; Rumelhart and Ingersoll, 1997; Blythe et al., 2000). Perhaps most striking are the differences between their topographic expressions. The San Gabriel Mountains are more thoroughly dissected and rugged than the San Bernardino Mountains, despite the similarities in basic form (Bull, 1991; Dibblee, 1975).

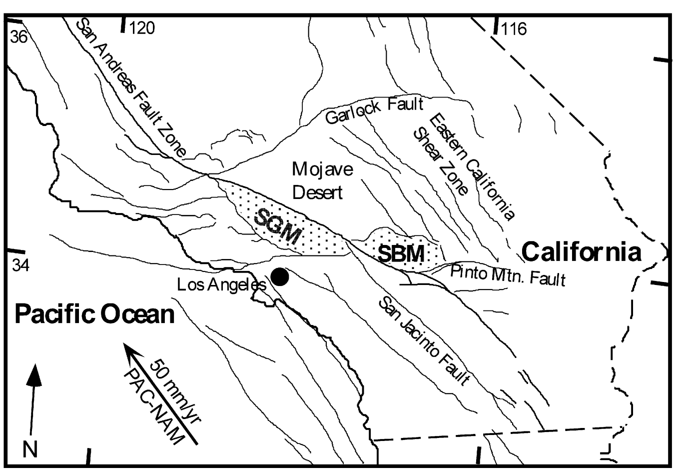

Figure 1. Simplified tectonic map of southern California. The location of the San Gabriel (SGM) and San Bernardino Mountains (SBM) are shown, along with major faults. The vector of Pacific-North American plate motion is also illustrated (DeMets, 1995).

The similarities and differences of these ranges create a unique opportunity to study the controls on erosion and topographic development of active mountain belts. Because the exhumation pattern of the Central Transverse Ranges is well constrained by geologic and thermochronometric data, it is possible to investigate variables that may control the geomorphic evolution of mountains by comparing their spatial distribution with established topographic and erosional trends. These adjacent, crystalline mountain ranges are broadly similar in their geography, deformation history, and climate, yet their geomorphology is quite distinct; why?

The erosion and landscape development of mountains are controlled by numerous factors. Erosion rates in mountain belts generally exhibit a positive correlation with relief or slope (Ahnert, 1970; Schumm, 1963; Pinet and Souriau, 1988; Burbank et al., 1996). This is consistent with slope-dependence of individual eroding agents, such as with fluvial incision (Whipple and Tucker, 1999; Hancock et al., 1999), bedrock landsliding (Densmore et al., 1997; Hovius et al., 1997) and glacial erosion (Paterson, 1994). Rock strength is also fundamentally important in controlling erosion rates and landforms (e.g., Weissel and Seidl, 1997), particularly in regions that experience bedrock landsliding (Schmidt and Montgomery, 1995) or in long-eroded orogens (Hack, 1960, 1982). Climate patterns further influence erosion. Greater precipitation leads to increased runoff and stream discharge that accelerate hillslope and fluvial erosion (Whipple and Tucker, 1999), increased ice flux that accelerates glacial erosion (Andrews, 1972), and increased ground saturation that leads to greater frequency of mass wasting events. Orographically controlled precipitation patterns can affect exhumation patterns and lead to asymmetric topography and flexural isostatic uplift (Weiland and Cloos, 1996; Willett, 1999; Masek et al., 1994). This influence has lead to coupled erosion-tectonic models, which predict that positive feedbacks between denudation and deformation lead to partitioning of tectonic uplift in mountain belts (e.g., Willett et al., 1993; Koons, 1995; Beaumont et al., 1992). A final control on topography and erosion in mountains is time. Davis (1899) expressed this as a theory of landscape maturity, in which uplifted mountain blocks retain preuplift landforms until they gradually erode and mature to a state of equilibrium. Although this theory has not survived intact (c.f. Hack, 1960), it cannot be denied that time is a major factor in the topographic development of mountains. This has been illustrated in both active (Tippet and Kamp, 1995) and extinct mountains (Baldwin et al., 2002).

To address these potential controls on erosion and geomorphic evolution of mountains, we have pooled existing geologic and thermochronometric data to create maps of long-term erosion rate in the Central Transverse Ranges. Although thermochronometry constrains only exhumation, we implicitly assume that the cooling of rocks in this case represents mainly the motion of rocks with respect to the geoid (rather than the motion of the earth's surface with respect to rocks) and erosion rather than tectonic denudation. These are reasonable assumptions, given the brief history of transpressive uplift and the lack of evidence for tectonic denudation in the San Gabriel and San Bernardino Mountains (Dibblee, 1975; Meisling and Weldon, 1989; Spotila et al., 1998; Blythe et al., 2000). The resulting maps of long-term erosion rate represent best-guess models that are in many cases speculative but which permit a comparison of erosion and topographic development with relevant parameters. We begin by exploring the topographic differences between the San Gabriel and San Bernardino Mountains and then describe the methodology used to estimate erosion rates. The patterns of erosion are then compared to variations in topography, deformation, bedrock, precipitation pattern, and time, both within and between the ranges, to gain a better understanding of what controls topography and erosion in mountains.

TOPOGRAPHY OF THE CENTRAL TRANSVERSE RANGES

It is remarkable how different the topographic expressions of the San Gabriel and San Bernardino Mountains are. The greater ruggedness and degree of incision of the San Gabriel Mountains are obvious on a small-scale digital elevation model (Fig. 2), as well as on any topographic map. These differences were described as early as 1907 by Mendenhall:

> The San Gabriel range has been completely dissected, resulting in thoroughly graded streams, sharp peaks, and knife-like ridges of discordant heights. No level areas at or near the summits, nor in the valley bottoms, exist with the mountain mass. The San Bernardino range contrasts sharply with its neighbor in these respects. Throughout its western end there is a strikingly level skyline at an elevation of 5000 feet or more. It contains many broad meadows, with lakes and playas, separated by smooth ridges. The topography of the central part is, in brief, topography of an old, well-reduced type. Several of the streams are not reduced to grade; they meander through broad uplands in the central part of the range, then plunge over falls into steep canyons, which they follow to the valleys that border the ranges.

A first order contrast between the topography of these ranges is apparent in their basic elevation and slope distribution. Elevation frequency in the San Gabriel Mountains increases steadily to a median of ~1275 m (average = 1351 m) and decreases rapidly to its 3070-m summit (Mount San Antonio; Fig. 3A). In contrast, elevation frequency in the San Bernardino Mountains is bimodally distributed, rising rapidly to a primary peak at ~1325 m, decreasing steadily, and then rising to a secondary peak at ~2075 m. This secondary peak presents a large area at high elevation that corresponds to the broad Big Bear plateau that spans the northern half of the range (Fig. 2). This high-altitude plateau is partly responsible for the greater average elevation of the San Bernardino Mountains (1616 m), although higher peak elevations (3506 m, Mount San Gorgonio) also contribute. Slope distribution in the two ranges is also distinct (Fig. 3B). Slopes are distributed broadly about a median of ~23° in the San Gabriel Mountains (average = 26°), whereas slope frequency in the San Bernardino Mountains has an asymmetric curve that peaks at ~15° (average = 17°). This asymmetry results from the high frequency of moderate to low slopes that occur across the Big Bear plateau and shows that the San Bernardino Mountains are less incised than the San Gabriel Mountains. Hypsometry also indicates this (Fig. 3C), as the lower curve of the San Gabriel Mountains corresponds to a lower hypsometric integral and implies greater dissection than in the San Bernardino Mountains (Strahler, 1952).

Contrast between the gentle Big Bear plateau and the more rugged San Gabriel Mountains is clear in east-west elevation profiles (Fig. 3D). The plateau is a broad, symmetric dome that exhibits only minor short-wavelength topography, whereas high-amplitude, short-wavelength undulations are common across the width of the San Gabriel Mountains. The San Gabriel Mountains also maintain a uniform peak height for some distance, but rise substantially on the east. North-south elevation profiles reveal other differences (Fig. 3E). The San Bernardino Mountains are dominated by two high ridges (Yucaipa Ridge, San Gorgonio massif) and the plateau, all of which are controlled by the position of major active faults. The San Gabriel Mountains are defined by a steep rise on the south and a gentle ramp on the north, but cannot be as easily subdivided into structural blocks and exhibit greater short-wavelength elevation variations. Faults do influence the San Gabriel Mountain's topography, although the valley along the San Gabriel fault may result from erosion of sheared rock rather than tectonic displacement.

These basic topographic features are also well defined on a map of slope distribution in the two ranges (Fig. 4). The San Gabriel Mountains exhibit steep slopes throughout their entire eastern half, although slopes decrease somewhat westward. The

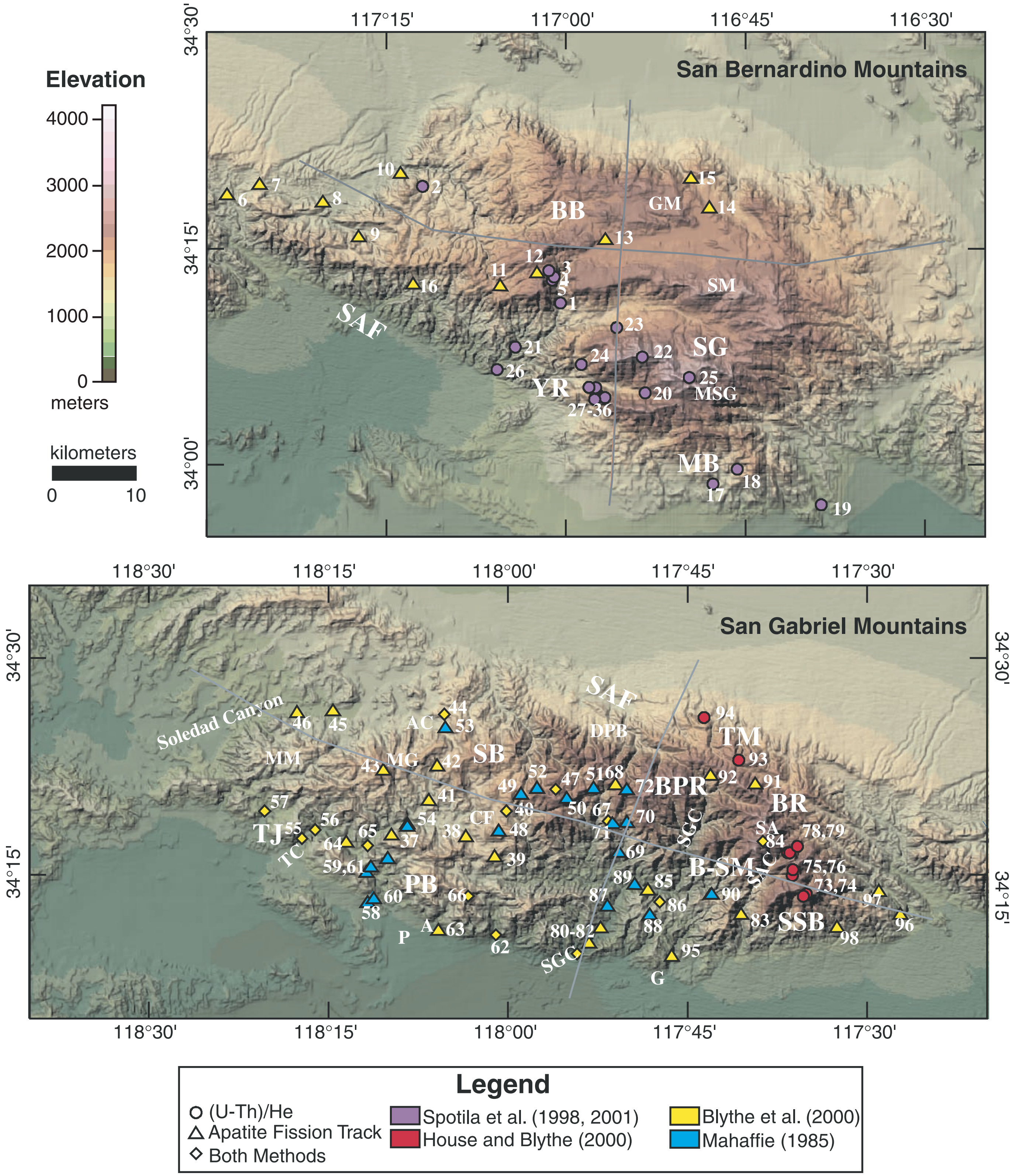

Figure 2. Digital elevation models of the San Gabriel and San Bernardino Mountains. These shaded relief maps are color-coded for elevation and based on 90 m resolution U.S. Geological Survey digital topography (color code based on "newrelief.aml" by Jeff Nighbert, B.L.M., Oregon). Locations of thermochronometric samples (1–99) tabulated in Table 1 are also shown (see Blythe et al., this volume, for a map with ages labeled). Lines show location of profiles in Figure 3. These are coded by source and type. Places names in the San Gabriel Mountains are abbreviated as; A—Altadena, AC—Aliso Canyon, BPR—Baden-Powell region, B-SM—Baldy-Sierra Madre block, DPB—Devils Punchbowl, G—Glendora, MG—Mount Gleason, MM—Magic Mountain, P—Pasadena, PB—Pasadena block, SA—San Antonio peak (3070 m), SAC—San Antonio Canyon, SAF—San Andreas fault, SB—Soledad block, SGC—San Gabriel Canyon, SSB—San Sevaine block, TC—Tujunga Canyon, TJ—Tujunga block, TM—Table Mountain. Place names in the San Bernardino Mountains are abbreviated as; BB—Big Bear plateau, GM—Gold Mountain, MB—Morongo block, MSG—Mount San Gorgonio (3506 m), SAF—San Andreas fault, SG—San Gorgonio Massif, SM—Sugarloaf Mountain, YR—Yucaipa Ridge block.

major strike-slip faults and range-bounding faults of the range are evident where steep mountain slopes meet gentle alluvial valleys. In contrast, slopes in the San Bernardino Mountains define topographic domains that correlate with structural blocks of variable exhumation history (Spotila et al., 1998). The gentle plateau is clearly defined and is bounded by steep northern and southern thrust-fault escarpments. The more rugged San Gorgonio and Yucaipa Ridge blocks are separated by low slopes in fault-controlled valleys to the south. Only in the southern San Bernardino Mountains are slopes as great as in the majority of the San Gabriel Mountains.

Geomorphic differences are also apparent in the drainage pattern of each range. The southern and northern margins of the San Bernardino Mountains are drained mainly by small basins that penetrate only a short distance into the range, with several exceptions (e.g., Santa Ana River; Fig. 5A). Along the wide eastern margin, larger elongate basins penetrate the range more effectively and drain radially away with an east-west fabric. In contrast, the central part of the range consists of the Deep Creek basin, which exhibits complex, meandering streams with gentle gradients that may reflect a palimpsest character (Sadler and Reeder, 1983). A portion of the Santa Ana basin (Bear Creek) may have formerly belonged to the Deep Creek basin and been captured from the south. This pattern suggests that a relict drainage networks drains the central plateau, while younger basins are encroaching from the perimeter of the range. In contrast, the San Gabriel Mountains are drained primarily by small, narrow peripheral basins that empty to the south (Fig. 5B). Exceptions to these include the San Gabriel and Tujunga basins, which drain large internal portions of the range, and several small basins that occur north of the divide between the Pacific Ocean and Mojave Desert. Both peripheral basins and stream networks draining the internal part of the range exhibit the same character and dendritic pattern, and thus give no hint of a palimpsest character. Lower drainage density and source density of streams in the San Gabriel Mountains also imply a lesser degree of drainage integration than in the San Bernardino Mountains (Fig. 5), although this could also reflect differences in relief or other boundary conditions. Drainage pattern in the two ranges is thus distinct and may reflect important differences in geomorphic evolution.

The main goal of this paper is to understand the origin of these geomorphic differences from the perspective of what controls erosion in the Transverse Ranges. Given that erosion is ultimately responsible for the character of topography, we address this problem by comparing spatial patterns of long-term erosion rate with the occurrence of relevant boundary conditions. Lifton and Chase (1992) investigated the relationship between deformation rate, rock type, and climate with topographic characteristics of small areas within the San Gabriel Mountains. We build on this work by investigating what controls long-term, large-scale erosion patterns in both ranges.

CONSTRAINING PATTERNS OF EROSION

Long-term erosion pattern in the San Bernardino Mountains

Abundant geologic and thermochronometric data constrain the pattern of erosion in the San Bernardino Mountains. Erosion magnitude over the past 2–3 m.y. is constrained across much of the range by a deeply weathered surface that represents a horizon of very low erosion. Where this surface is absent, rapid exhumation has taken place that is constrained by thermochronometry (Spotila et al., 1998; Blythe et al., 2000; Spotila et al., 2001). Because the weathered surface is such an important constraint, we discuss its character and the arguments for its origin in detail.

Distributed atop the Big Bear plateau and isolated locations atop the San Gorgonio block are remnants of a deeply weathered granitic surface. This surface represents a mappable geologic feature that bears characteristics typical of deep granitic weathering (e.g., Mabbutt, 1965; Ollier, 1975). Its hummocky surface displays low relief (<100 m over short wavelengths; typical slopes of ~6°) and is mantled by thick granitic saprolite (Spotila, 1999). Fresh granitic bedrock, exposed in canyons incised into the plateau, grades upwards into an accumulation of resistant core-stones surrounded by a disaggregated skeletal matrix of grus. Well-developed soil horizons are locally preserved atop this saprolite. These are commonly brick-red (10R3/4), argillaceous (Bt horizons are typically ~20% clay, but locally as much as 47% clay [Spotila, 1999]), show extreme mineral decay, and formed in situ from a quartz monzonite parent that forms the majority of the plateau. Weathered debris is locally >30 m thick (Spotila, 1999; Brown, 1976), although more typically soil and saprolite have been scraped away to expose interlocking core-stones as resistant inselbergs. These characteristics are common of weathering in humid climates (e.g., Brazil [Power and Smith, 1994], Guayana [Eden, 1971], Sierra Leone [Teeuw et al., 1994]; Virginia [Pavich, 1986], England [Williams et al., 1986]). Nongranitic rocks atop the plateau consistently protrude above the weathered surface as isolated highs, such as Onyx Peak (quartzite) and Shay (quartzite), Gold (quartzite and marble), Sugarloaf (quartzite), and White (quartzite and marble) Mountains. These monadnocks display low relief and are generally capped by deep-red colluvium. The average elevation of quartz monzonite atop the plateau is 420 m lower than quartzite bedrock, suggesting significant differential weathering and erosion (Spotila, 1999). This is another common attribute of weathered granite in warm, humid climates (e.g., etchplanation is ~400 m in Sierra Leone [Teeuw et al., 1994] and ~300 m in Hong Kong [Ruxton and Berry, 1957]).

If the weathered surface of the San Bernardino Mountains and adjacent Mojave Desert formed in a humid climate distinct from the present Mediterranean climate, it may be relict from the Miocene when precipitation was significantly greater (Ax-

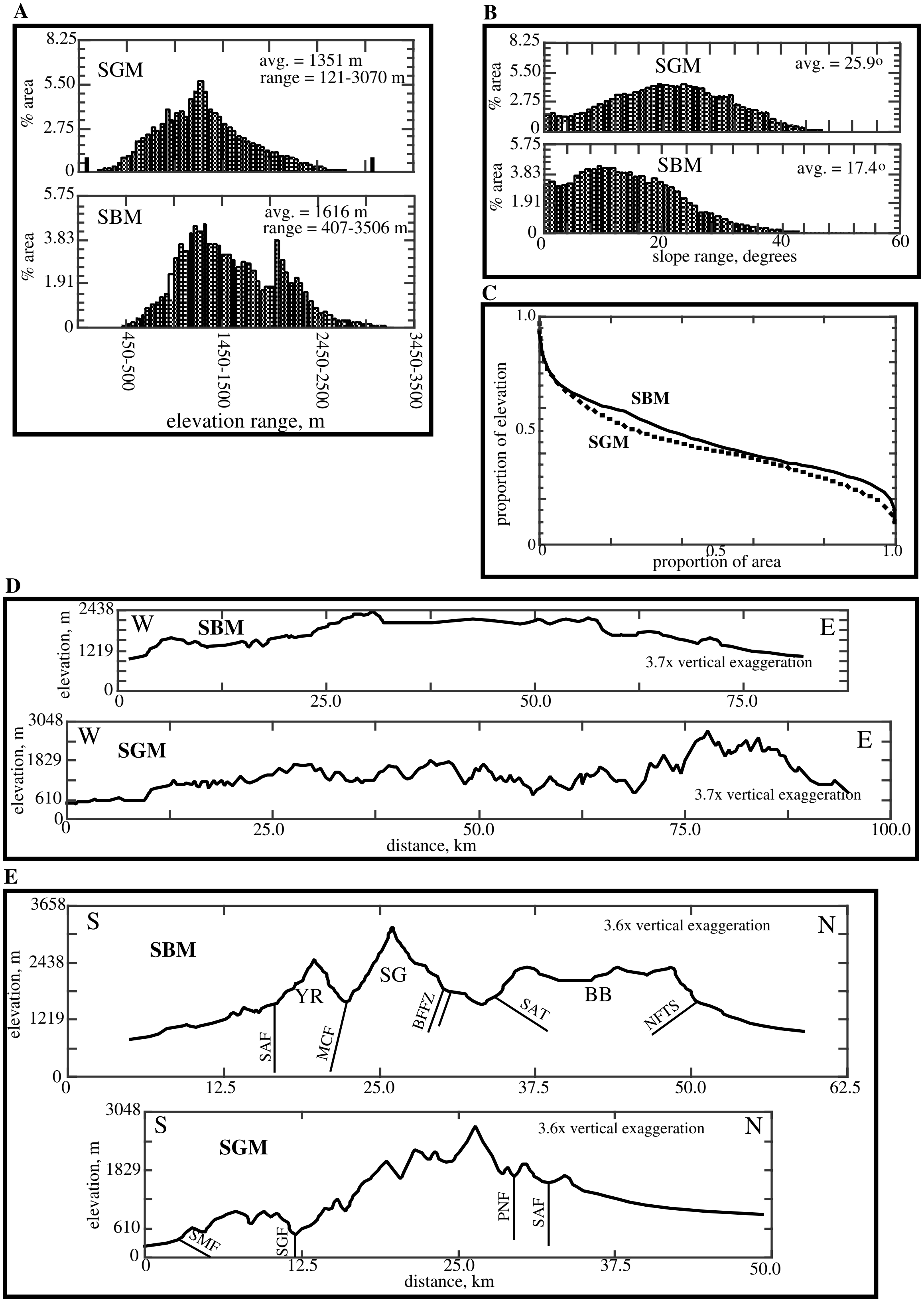
A
SGM
avg. = 1351 m
range = 121-3070 m
SBM
avg. = 1616 m
range = 407-3506 m
% area
elevation range, m
450-500
1450-1500
2450-2500
3450-3500
B
SGM
avg. = 25.9°
SBM
avg. = 17.4°
% area
slope range, degrees
C
SBM
SGM
proportion of elevation
proportion of area
D
W
E
SBM
SGM
3.7x vertical exaggeration
elevation, m
distance, km
E
S
N
SBM
SGM
3.6x vertical exaggeration
YR
SG
BB
SAF
MCF
BFFZ
SAT
NFTS
SMF
SGF
PNF
elevation, m
distance, km

Figure 3. Comparison of topography in the San Gabriel (SGM) and San Bernardino (SBM) Mountains. A: Distribution of elevation in the two ranges. Elevations from 90 m resolution digital elevation models covering each range (as defined by alluviated perimeters of each range) were binned at 50 m intervals and plotted versus percent area. The San Gabriel Mountains only includes the portion of the range that extends southeast of Soledad Canyon (Fig. 2). B: Distribution of slope in each range, including the San Gabriel Mountains southeast of Soledad Canyon. Slopes were calculated using the program *Arc/Info* on 90-m resolution digital topography for each range, binned in one-degree intervals and plotted versus area. Average slopes in the San Gabriel Mountains are comparable to the results of Blythe et al. (2000) using 30 m digital topography. C: Hyposometric curves (Strahler, 1952) of elevation frequency the two ranges, including the San Gabriel Mountains southeast of Soledad Canyon, calculated with *Arc/Info*. D: Elevation profiles from west to east in each range constructed from 1:250 000 scale topographic maps. Location of profiles are shown in Figure 2. E: Elevation profiles from south to north in each range. BB—Big Bear plateau, BFFZ—Barton Flats fault zone, MCF—Mill Creek fault, NFTS—North Frontal thrust system, PNF—Punchbowl-Nadeau fault, SAF—San Andreas fault, SAT—Santa Ana thrust, SG—San Gorgonio block, SGF—San Gabriel fault, SMF—Sierra Madre fault, YR—Yucaipa Ridge.

elrod, 1950; Oberlander, 1972). However, similar granitic weathering has been described in arid regions (e.g., Corsica; Power and Smith, 1994), suggesting this need not be the case. In addition, deep chemical weathering can be facilitated by local hydrology, vegetation, bedrock characteristics, and other factors, making it difficult to conclude that this weathered surface must be relict. Nonetheless, a strong argument can be made that this surface represents a horizon that has been little-modified by erosion since uplift initiated 2–3 Ma. Rates of granitic saprolite formation in tropical locations are typically less than ~0.1 mm/yr and more commonly closer to ~0.02 mm/yr (Edmond et al., 1995; Saunders and Young, 1983), while rates in humid temperate locations can be even lower (<0.01 mm/yr; e.g., Pavich, 1986; Williams et al., 1986). Denudation rates of subaerial granitic inselbergs along similar weathered surfaces have been observed as low as 0.0004 mm/yr (Bierman and Turner, 1995). Thus, even if saprolite atop the Big Bear plateau formed at a rapid rate of granite weathering, its total thickness would have required more than a million years of sustained chemical weathering in the absence of erosion to accumulate.

Additional support for this argument comes from local onlapping relationships. On the eastern flank of the range (Fig. 6A), from the floor of the Mojave to an elevation of ~2 km atop the plateau, remnants of 6–9 Ma basalt flows are preserved atop the weathered surface (Neville and Chambers, 1982; Oberlander, 1972; Woodburne, 1975). Where preserved, these basalts mark horizons of nearly zero synorogenic erosion. Between correlative flows, the depth of incision averages only 130–145 m, implying a maximum post-Miocene erosion rate of 0.014–0.024 mm/yr (Spotila, 1999). The central plateau surface, which is less incised than the surface on the eastern flank (e.g., Pipes Creek, Morongo Creek), may have experienced even slower rates of post-Miocene erosion. Other preuplift deposits that cap the surface and constrain its age include the late Miocene–Pliocene Old Woman Sandstone north of in the Mojave Desert and the middle to late Miocene Crowder Formation in the western wing of the plateau (Meisling and Weldon, 1989). Both the Crowder Formation and the weathered surface are cut by strands of the late Miocene Cedar Springs reverse fault system (Meisling and Weldon, 1989). Deeply weathered granite also occurs beneath exposures of late Miocene Santa Ana Sandstone in the Santa Ana Valley (Jacobs, 1982; Sadler, 1993). Although mappable upper Tertiary deposits are not present across the central portion of the plateau and San Gorgonio massif, gravels of possible preorogenic origin occur sporadically there (Fig. 6A and 7A). These undated deposits consist of loose assortments of large, rounded cobbles that include distinctive quartzite derived from Sugarloaf or Gold Mountain (Fig. 2; Sadler and Reeder, 1983). Many of these gravels are perched on ridges and hills high above modern trunk streams and could not have been deposited by the present drainage network. Gravels on the eastern flank of the plateau contain volcanic clasts derived from the Mojave Desert near Victorville, indicating a preuplift origin (Sadler and Reeder, 1983). Although these gravels could have been recycled, they support the idea that the central plateau has experienced minimal erosion.

Minimal syn-uplift erosion of the plateau and San Gorgonio massif is further indicated by (U-Th)/He and fission track dating in the range. Helium ages from the weathered surface are old (ca. 65 Ma) and indicate that less than ~2 km of exhumation occurred throughout the Tertiary (Table 1; Spotila et al., 1998). We calculated long term exhumation rates from these ages by assuming closure temperatures of 70 °C for helium and 110 °C for fission tracks, a geothermal gradient of 30 °C/km, ambient surface temperature of 10 °C, and ignoring the effects of topography and advection on the geometry of isotherms (Mancktelow and Grasemann, 1997) (Table 1). These rates vary from 0.03–0.07 mm/yr and are consistent with slow exhumation in the Cenozoic. Given the likelihood that a period of rapid cooling occurred at the end of the Cretaceous, rocks from the plateau surface may have experienced even lower exhumation rates or prolonged crustal stasis (Spotila et al., 1998). Below the weathered surface helium ages decrease rapidly with elevation (Table 1). Exhumation rate inferred from this steep age-elevation gradient is ~0.02 mm/yr, although the age-elevation relationship may also represent and exhumed helium partial retention zone (Spotila et al., 1998). An important feature of these data are that ages are essentially invariant across the weathered surface, despite an elevation span of ~1–2 km (Table 1). This is true for ages measured from samples at or just below the weathered surface atop the San Gorgonio block as well, supporting the idea that its locally-preserved weathered surface correlates with that atop the plateau (Spotila et al., 1998). In all cases, the weathered surface appears to represent a marker horizon that parallels helium isochrons, tilting downwards to the

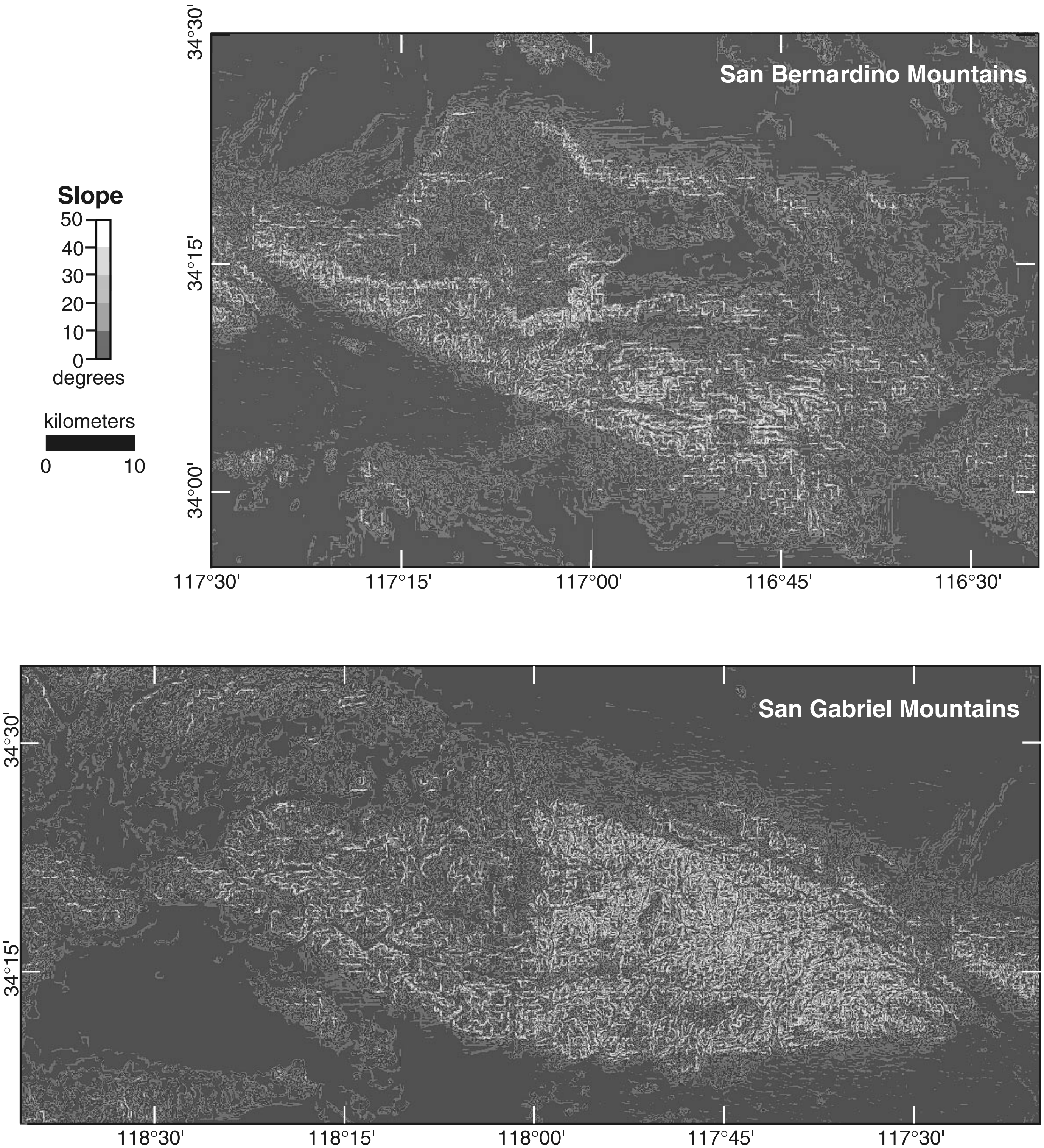

Figure 4. Map of slopes in the San Gabriel and San Bernardino Mountains, based on slopes calculated with *Arc/Info* using 90 m scale digital topography. Slopes are gray-shade coded for values in degrees. Refer to Figure 2 for locations of blocks and Figure 6 for locations of major structures.

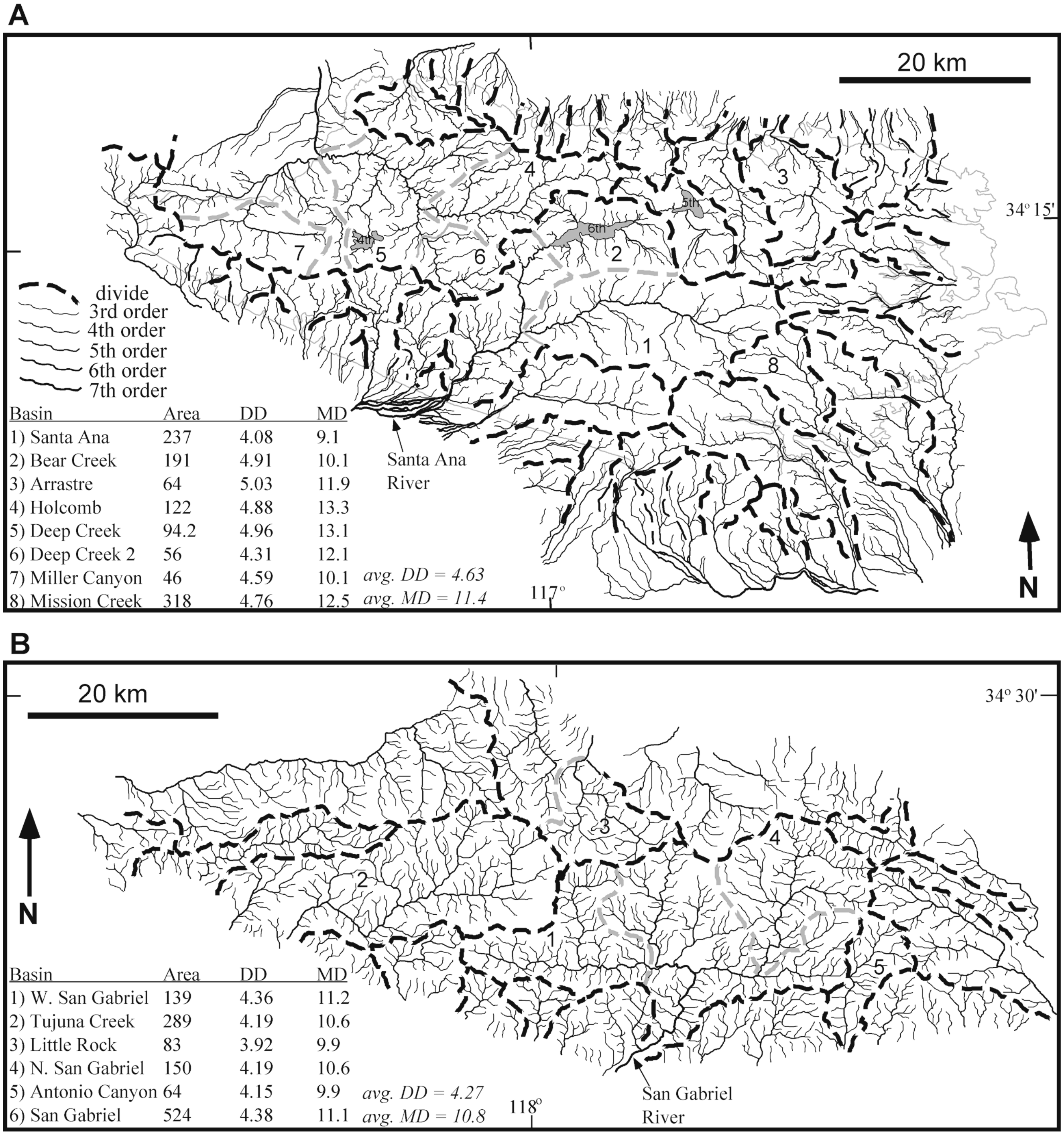

Figure 5. A: Drainage map of the San Bernardino Mountains, compiled from streams mapped from 1:62,500 scale topographic maps. Streams are line-width coded for Strahler order, based on determination from the original maps, but only streams of 3rd order or higher are shown. Lakes are shown and labeled for the order that a stream would have if present instead (e.g., artificial Big Bear Lake has two 5th order streams entering it and is thus labeled 6th order; Bear Creek that continues below Big Bear dam is also 6th order). Drainage divides are shown as heavy dashed lines. Heavy gray dashed lines define subdivisions of basins used for calculations of drainage parameters listed in the table. These parameters, including basin area (in km^2), drainage density (DD, in km/km^2), and magnitude density (MD, in number of junctions per km^2) were calculated for the basin areas indicated by number. These calculations were made using the software *Rivertools* on drainages calculated from 30 m resolution digital elevation models. The irregular arrangement of basins used for these calculations resulted from errors in the digital elevation models that made some areas unusable. B: Drainage map of the San Gabriel Mountains, drawn from 1:250 000 scale topographic maps. Stream are shown with similar line-width scaling as in Figure 5A, but exact stream orders are indetermined due to the smaller topographic scale used. Increases in line thickness therefore represent increases in relative Strahler order. Parameters for the numbered reaches of basins are listed in the table and calculated as in Figure 5A.

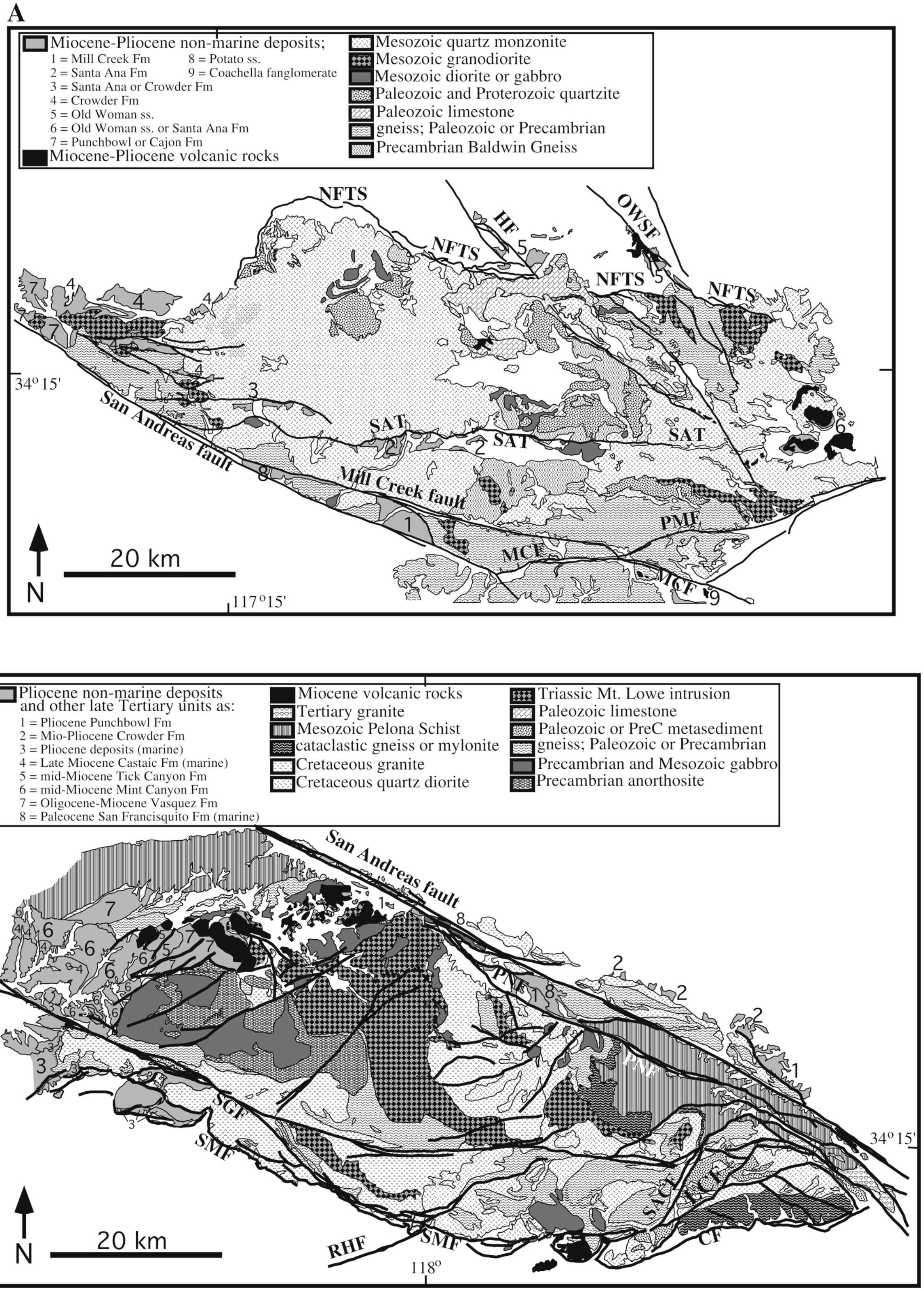

Figure 6. A: Geologic map of the San Bernardino Mountains reproduced from the 1:250 000 compilation of Bortugno and Spittler (1986). Miocene-Pliocene units are labeled by formation with the numbers indicated (Proctor, 1968; May and Repenning, 1982; Meisling and Weldon, 1989; Sadler, 1993; Sadler et al., 1993). Major faults are indicated. HF—Helendale fault, MCF—Mission Creek fault, NFTS—North Frontal thrust system, OWSF—Old Woman Springs fault, PMF—Pinto Mountain fault, SAT—Santa Ana thrust. B: Geologic map of the San Gabriel Mountains reproduced from the 1:250 000 compilation of Jennings and Strand (1969). Tertiary units are labeled by formation with the numbers shown (Dibblee, 1982a; Crowell, 1982; Treiman, 1982; Weigand, 1982; Ehlert, 1989; Dibblee, 1987). Major faults are included. CF—Cucamonga fault, LCF—Southfork Lytle Creek fault, PNF—Punchbowl-Nadeau fault, RHF—Raymond Hill fault, SACF—San Antonio Canyon fault, SGF—San Gabriel fault, SMF—Sierra Madre fault.

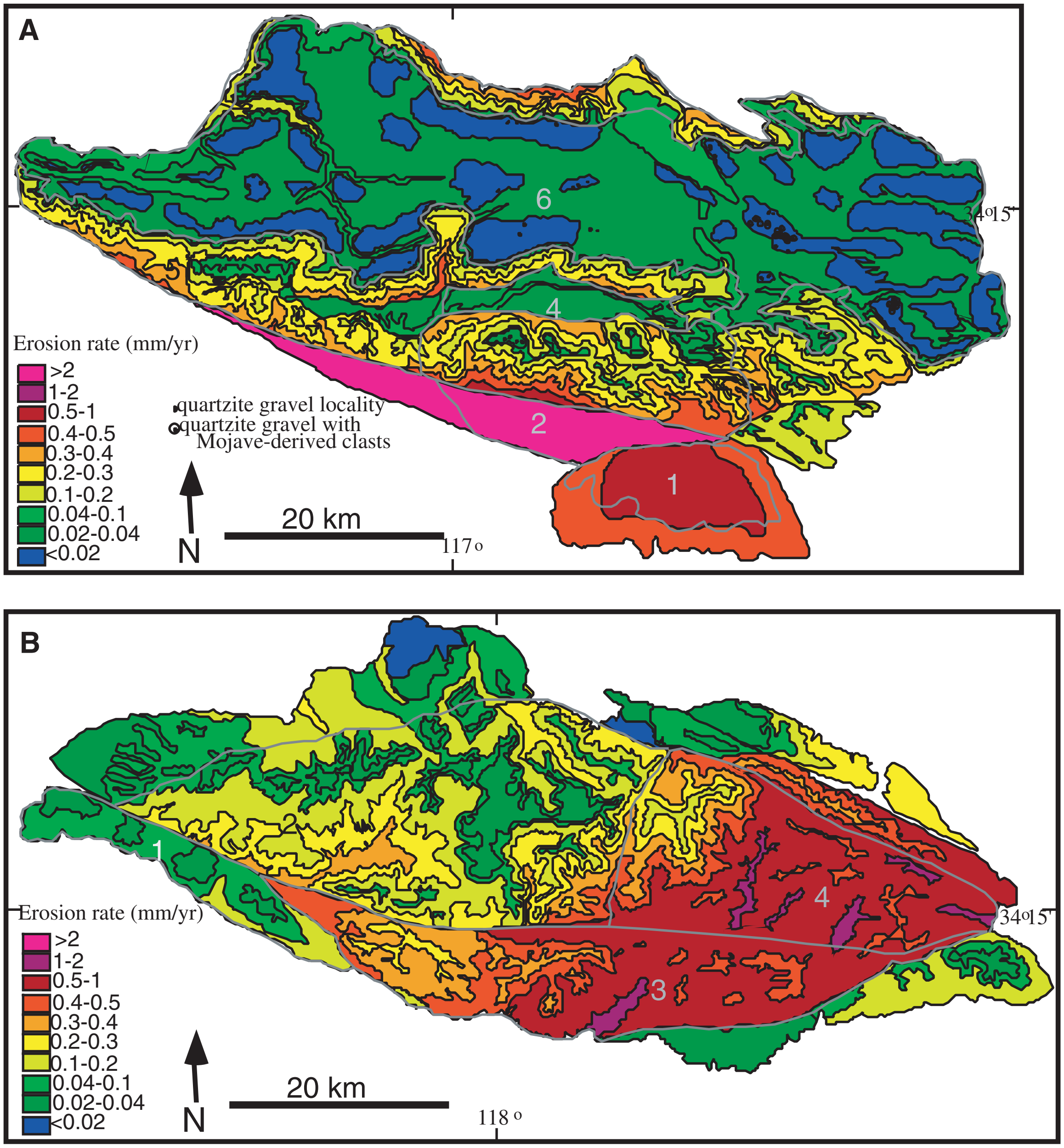

Figure 7. A: Map of average erosion rates in the San Bernardino Mountains since their initiation of uplift 2.5 Ma. Rates were estimated from available thermochronometric and geologic constraints as described in text. The locations of quartzite gravels, which are an important constraint for erosion atop the Big Bear plateau, are also shown (Sadler and Reeder, 1983). Light gray lines define the seven topographic domains on which average erosion rates were computed and compared to average slope and elevation in Figure 8 (1—Morongo block; 2—Yucaipa Ridge block; 3—San Gorgonio block; 4—Santa Ana Valley; 5—San Bernardino range front; 6—Big Bear plateau; 7—north frontal range front). B: Map of average erosion rates in the San Gabriel Mountains since their inception of uplift 6 Ma. Rates were estimated using data as described in the text. Outlines of four topographic domains used in Figure 8 are shown (1—Tujunga block; 2—Western block; 3—Sierra Madre block; 4—Baldy block).

east and west atop the plateau and defining a gentle antiform in the San Gorgonio massif.

We used the weathered surface as a marker horizon to constrain erosion from the top of the Big Bear plateau (Fig. 7A). We assume this surface experienced <100 m total erosion during uplift of the range, so that where it is preserved we infer a long-term average erosion rate over the life span of the San Bernardino Mountains (ca. 2.5 Ma) of <0.04 mm/yr. Along the most pristine, low-relief portions of the surface and where late Miocene deposits or quartzite gravels overlie it, we assume

TABLE 1. APATITE HELIUM AND FISSION TRACK DATA FROM THE CENTRAL TRANSVERSE RANGES

Number	Sample ID*	AFT age[†]	He age[§]	Elevation (m)	ER FT[#]	ER HE**	Source[‡]
San Bernardino Mountains; Big Bear block							
1	SBHe7		20.6	1233		0.10	(1)
2	SBHe10		51.2	1329		0.04	(1)
3	SBHe15		49.4	1614		0.04	(1)
4	SBHe16[§§]		52.4	1812		0.04	(1)
5	SBHe17[§§]		64.3	2113		0.03	(1)
6	SB1[§§]	53.6		980	0.06		(2)
7	SB2[§§]	56.8		1130	0.06		(2)
8	SB3[§§]	60.2		1050	0.06		(2)
9	SB4[§§]	54.9		1200	0.06		(2)
10	SB5[§§]	57.1		1390	0.06		(2)
11	SB7[§§]	58.2		1875	0.06		(2)
12	SB8[§§]	54.4		2130	0.06		(2)
13	SB9[§§]	90.9		2070	0.04		(2)
14	SB10	45.5		1970	0.07		(2)
15	SB11[§§]	70.4		1550	0.05		(2)
16	SB22[§§]	57.4		1080	0.06		(2)
San Bernardino Mountains; Morongo block							
17	DYJS6		5.2	981		0.38	(3)
18	DYJS7		4.5	1333		0.44	(3)
19	DYJS9		12.6	556		0.16	(3)
San Bernardino Mountains; San Gorgonio block							
20	SBHe12	63	14.3	1526	0.05	0.14	(1,6)
21	SBHe20	43	18.2	756	0.08	0.11	(1,6)
22	SBHe24[§§]		52.6	3311		0.04	(1)
23	SBHe25		40.8	1861		0.05	(1)
24	SBHe26		14.5	1899		0.14	(1)
25	SBHe27[§§]		55.7	3506		0.04	(1)
San Bernardino Mountains; Yucaipa Ridge/Wilson Creek block							
26	SBHe19		0.7	652		2.86	(1)
27	SBHe21		1.6	2323		1.25	(1)
28	SBHe23		1.6	1387		1.25	(1)
29	DYJS1		1.5	2060		1.33	(3)
30	DYJS2		1.6	1908		1.25	(3)
31	DYJS3		1.4	1768		1.43	(3)
32	DYJS4		1.4	1658		1.43	(3)
33	DYJS5		1.4	1506		1.43	(3)
34	SBHe21		1.5	2323		1.33	(3)
35	SBHe22		1.6	1969		1.25	(3)
36	SBHe23		1.4	1387		1.43	(3)
San Gabriel Mountains; Soledad region							
37	SG20	16.1		990	0.21		(2)
38	SG21	48.4		1170	0.07		(2)
39	SG22	36.3		1520	0.09		(2)
40	SG23	43.6	42.8	1620	0.08	0.05	(2)
41	SG24	63.6		1070	0.05		(2)
42	SG25	38.3		1280	0.09		(2)
43	SG26	51.2		1680	0.07		(2)
44	SG27	37.1	23.2	1220	0.09	0.09	(2)
45	SG28	42.1		700	0.08		(2)
46	SG29	27.9		650	0.12		(2)
47	SG38	40.9	40.6	2140	0.08	0.05	(2)
48	TR9	42.7		1628	0.08		(4)
49	TR10	38.3		1803	0.09		(4)
50	TR11	44.5		2146	0.07		(4)
51	TR12	35.9		2060	0.09		(4)
52	TR17	53.1		1939	0.06		(4)
53	MTR30	55.3		1268	0.06		(4)
54	TR3	51.9		838	0.06		(4)

(*continued*)

TABLE 1. APATITE HELIUM AND FISSION TRACK DATA FROM THE CENTRAL TRANSVERSE RANGES (continued)

Number	Sample ID*	AFT age[†]	He age[§]	Elevation (m)	ER FT[#]	ER HE**	Source[‡]
San Gabriel Mountains; Tujunga block							
55	SG3	47.7	33.3	470	0.07	0.06	(2)
56	SG4	51.2	34.6	530	0.07	0.06	(2)
57	SG19	59.5	42.4	520	0.06	0.05	(2)
58	TR1	42.9		512	0.08		(4)
59	MTR26	57.6		975	0.06		(4)
60	TR19	34.1		597	0.10		(4)
61	MTR28	51.8		896	0.06		(4)
San Gabriel Mountains; Pasadena block							
62	SG1	11.8	6.6	270	0.28	0.30	(2)
63	SG2	26.7		350	0.12		(2)
64	SG5	6.1		560	0.55		(2)
65	SG6	10.0	3.1	670	0.33	0.64	(2)
66	SG7	11.9	7.6	1710	0.28	0.26	(2)
San Gabriel Mountains; Baden Powell region							
67	SG33	19.3	8.9	1700	0.17	0.23	(2)
68	SG37	14.2		2050	0.23		(2)
69	MTR6	38.3		804	0.09		(4)
70	MTR8	40.4		1524	0.08		(4)
71	MTR9	31.6		1600	0.11		(4)
72	TR13	43.8		2141	0.08		(4)
San Gabriel Mountains; Baldy/Sierra Madre block							
73	99MHCP1		5.4	2533		0.37	(5)
74	99MHCP3		5.2	2620		0.38	(5)
75	MH99TP1		10.9	2131		0.18	(5)
76	MH99TP2a		5.7	2657		0.35	(5)
77	MH99TP3a		6.8	2380		0.29	(5)
78	SG40		6.0	2383		0.33	(5)
79	SG42	3.0	1.8	2019	1.11	1.11	(5,6)
80	SG8	5.3	6.3	230	0.63	0.32	(2)
81	SG9	3.0		350	1.11		(2)
82	SG10	4.5		419	0.74		(2)
83	SG11	8.4		980	0.40		(2)
84	SG12	7.0	5.1	3070	0.48	0.39	(2)
85	SG30	9.0		500	0.37		(2)
86	SG31	13.0	6.8	820	0.26	0.29	(2)
87	MTR4	33.9		500	0.10		(4)
88	MTR12	31.8		975	0.10		(4)
89	MTR10	33.7		488	0.10		(4)
90	MTR11	29.7		671	0.11		(4)
San Gabriel Mountains; Blue Ridge/Table Mountain							
91	SG35	8.6		2150	0.39		(2)
92	SG36	3.7		2100	0.90		(2)
93	TableMtn1a	8	10.4	2008	0.42	0.19	(5,6)
94	TableMtn2a	42	19.2	1381	0.08	0.10	(5,6)
San Gabriel Mountains; San Sevaine block							
95	SG14	40.4		470	0.08		(2)
96	SG16	18.2		700	0.18		(2)
97	SG17	42.3		840	0.08		(2)
98	SG39	32.7		1022	0.10		(6)

*Sample ID—published sample name, # refer to Figure 2 (for map with ages labeled, see Blythe et al., this volume).

[†]AFT Age—apatite fission track age.

[§]He age—(U-Th)/He age.

#ER FT—inferred exhumation rate for fission track age (closure temperature = 70C, geothermal gradient = 30C/km, surface temp. = 10C).

**ER HE = inferred exhumation rate for helium age (closure temperature = 70C, geothermal gradient = 30C/km, surface temp. = 10C). Geothermal gradient based on Wright (1987).

‡Sources: (1) Spotila et al. (1998), (2) Blythe et al. (2000), (3) Spotila et al. (2001), (4) Mahaffie (1985), (5) M. House (2001, written commun.), (6) Blythe (2001, written commun.).

[§§]Samples at or just below the weathered surface.

rates have been somewhat less (<0.02 mm/yr). Where thick late Miocene deposits have been heavily incised, such as in the structurally low Santa Ana Valley between the massif and plateau, we assume a slightly higher rate (0.04–0.02 mm/yr). Where the weathered surface is absent across these blocks, notably in canyons or along northern and southern escarpments, we calculate average erosion rate by finding the elevation difference between present topography and the projected position of the missing weathered surface above. For example, the base of the range along its northern front is locally ~1.3 km in elevation, or ~1.1 km below the weathered surface atop the rim of the plateau above. To account for erosion the plateau may have experienced, we add 100 m to this difference and find an average erosion rate of 0.48 mm/yr (i.e., 1.2 km/2.5 Ma). This assumes a horizontal structural envelope from the rim of the plateau to above the traces of the bounding thrust faults, but provides an estimate of erosion rate along the entire northern and southern plateau escarpments. Erosion rates for the San Gorgonio block are calculated in a similar way, but the projected structural envelope is not assumed to be horizontal. Instead, the broad north-plunging antiformal shape is used, as defined by helium isochrons and remnants of the weathered surface (Spotila et al., 1998). As a result, erosion rates for ridges and peaks do not get higher than 0.2 mm/yr, although elevations decrease from 3.5 km in the center to <1.5 km on the east and west (Fig. 2).

For blocks trapped within the San Andreas fault zone that do not preserve the weathered surface or late Miocene deposits, such as the Yucaipa Ridge and Wilson Creek blocks, we rely on estimates of exhumation from (U-Th)/He dating. Young (ca. 1.5 Ma) apatite helium ages from these blocks imply up to 6 km of exhumation in a short interval (ca. 1.8–1.0 Ma; Spotila et al., 2001), but averaged >2.5 m.y. imply an average erosion rate of ~2.8 mm/yr. Ignoring the potential effect of isotherm advection associated with rapid exhumation, which is likely to be minor given the narrow width of these blocks (Spotila et al., 2001), we assign average erosion rates of >2 mm/yr to these blocks (Fig. 7A). Note that exhumation rates reported on Table 1 are lower than this, because they do not take into account the higher closure temperatures associated with rapid rates of cooling (Wolf et al., 1996; Farley, 2000). Also note that these rates imply significant basin inversion of the well-lithified, middle Miocene Mill Creek Formation and Potato Sandstone (Sadler et al., 1993), which occur in fault contact with the Yucaipa Ridge block and depositional contact with the Wilson Creek block (Fig. 6A).

For the Morongo block, we estimate long-term erosion using both (U-Th)/He dating and the presence of preorogenic deposits. Apatite helium ages of 4–5 Ma at ~1 km elevation on the west imply average, post–late Miocene exhumation at ~0.4 mm/yr (Table 1). Based on sedimentary facies of the Pliocene marine Imperial Formation (Murphy, 1986) and provenance of the Mount Eden and San Timoteo Formations further west (Reynolds and Reeder, 1986; Albright, 1999), however, it is likely that uplift and erosion did not begin until after 2–3 Ma. This doubles the assumed erosion rate (i.e., 2 km exhumed in 2.5 Ma; 0.8 mm/yr). A slightly older helium age (13 Ma) on the far west implies that erosion rates decrease toward the block perimeter (Table 1, Fig. 7A), consistent with the structural interpretation of the block as a broad dome (Yule and Sieh, 2002). Adopting this interpretation, we assign a rate of 0.4 mm/yr for the perimeter. This is the same rate as where ~1 km of erosion has occurred below the weathered surface in the Big Bear block, where helium ages are about the same (ca. 14–21 Ma; Table 1). Miocene deposits occur around the perimeter of the dome, such as the Coachella Fanglomerate and Imperial Formation, but these are separated by faults and overridden by crystalline rock and thus aren't used for estimated erosion rates (Allen, 1957; Proctor, 1968).

Based on the resulting pattern (Fig. 7A), the spatially averaged long-term erosion rate in the San Bernardino Mountains during the past ~2.5 m.y. has been ~0.28 mm/yr. This is slightly higher than determined from restoration of the weathered surface by Spotila and Sieh (2000), because of the greater detail in our analysis and the higher erosion rates used for several blocks that are implied by new data (Spotila et al., 2001). The pattern of erosion rates is fairly well constrained, given the volume of data used. Although details may require modification as new data are collected, such as along the southeastern flank of the range, the broad pattern is robust. However, given the large number of assumptions required to generate this pattern, Figure 7A should be viewed as a best-guess, nonunique interpretation. Given the complexity in generating this pattern, it is also very difficult to estimate uncertainties. In some areas, uncertainties in helium ages or assumed geothermal gradients, the effect of nonhorizontal isotherms or thermal advection, and other factors may lead to large uncertainty in estimated erosion rate (~50%?). In other areas, the uncertainty may be considerably less. Given the comparative nature of this study, however, we have not performed a rigorous analysis of errors.

Erosion pattern in the San Gabriel Mountains

The pattern of erosion in the San Gabriel Mountains is constrained by similar thermochronometric and geologic data. As in the San Bernardino Mountains, we estimate average, long-term erosion rates that span the entire duration of uplift, which we assume to be ~6 m.y. (Rumelhart and Ingersoll, 1997; Blythe et al., 2000). Because the San Gabriel Mountains have experienced a longer period of construction, equal rates of erosion in these mountains are of course associated with more than double the total denudation than in their younger counterpart. Although estimating erosion rates averaged over the duration of uplift provides a basis for comparison to various parameters, the degree to which the difference in uplift history has affected their geomorphic evolution is explored in detail later.

Tertiary deposits provide local constraint on erosion history of the San Gabriel Mountains. Along the western portion of the range at Soledad Canyon, the upper Miocene Mint Canyon Formation onlaps crystalline basement (Fig. 6B). This unit consists of fluvial and lacustrine facies and overlies gneiss and anorthosite, thereby indicating previous exposure and thus minimal recent unroofing of basement (Dibblee, 1982a; Crowell, 1982; Ehlert, 1989). Other Tertiary units of the San Gabriel Mountains west of Soledad Canyon also imply previous subsidence and limited syn-orogenic (post–6 Ma) denudation, including the Miocene nonmarine Tick Canyon Formation, upper Miocene marine Castaic Formation, Oligocene nonmarine, volcanic-rich Vasquez Formation, thick graben-fill of the Ridge Basin Group along the San Gabriel fault, and the lower Tertiary to Quaternary, marine and nonmarine units (Topanga, Modelo, Elsmere, and Saugus Formations) of the Ventura basin south of the San Gabriel fault (Crowell, 1982; Dibblee, 1982a; Treiman, 1982; Weigand, 1982; Ehlert, 1989). In the south-central San Gabriel Mountains, the Miocene (?) Glendora Volcanics, locally overlain by the Puente Formation, overlie basement and indicate minimal erosion of fault slices that occur south of several major structures (Weigand, 1982). In the north-central part of the range between strands of the San Andreas fault, the Paleocene-Eocene marine San Francisquito Formation and upper Miocene terrestrial Punchbowl Formation overlie a basement surface in the Devil's Punchbowl, also limiting local erosion (Dibblee, 1987).

These constraints provide slightly less resolution on the pattern of erosion in the San Gabriel Mountains than the weathered surface provides in the San Bernardino Mountains. The lack of a deeply weathered surface in the San Gabriel Mountains may actually be due to greater total exhumation than the San Bernardino Mountains have experienced. As a result of the poorer resolution, the thermochronometry holds a more critical role in defining erosion patterns of the San Gabriel Mountains. We calculate exhumation by applying the same techniques and assumptions as for the San Bernardino Mountains on abundant apatite fission track and (U-Th)/He ages. We reply primarily on data from Blythe et al. (2000) and House (written commun.), although fission track ages from Mahaffie (1985) provide additional local constraint (Fig. 2; Table 1).

For isolated locations where Tertiary deposits overlie basement, including southern and northern Soledad Canyon and the Devil's Punchbowl, we assign an average erosion rate of <0.02 mm/yr. At this rate, ~120 m of erosion would have occurred in the past 6 m.y. This may underestimate the vertical thickness of Tertiary units that have been eroded from some of these exposures, but a palinspastic reconstruction of missing sediments and volcanic units was beyond the scope of this study. The low rate we have inferred cautiously illustrates how preservation of these late Tertiary units required minimal unroofing of basement during recent uplift. For the basement overlain by the older Glendora Volcanics in the south, we arbitrarily assigned a higher rate of 0.02–0.04 mm/yr.

Proceeding southeast of Soledad Canyon into a region we define as the Soledad and Tujunga blocks, the range rises into a series of broad, moderately subdued ridges, such as near Magic Mountain and Mount Gleason (Fig. 2). The topographic ruggedness of this region is less than in the easternmost San Gabriel Mountains (Fig. 4). Apatite fission track and helium ages from these blocks are also the oldest found in the range, clustering near ca. 40 Ma but as old as 64 Ma (Table 1). Similarity between fission track and helium ages implies rapid cooling from ~110–70 °C and argues that less than ~2 km of exhumation has occurred since ca. 40 Ma, implying average exhumation rates for the middle to late Tertiary of ~0.05 mm/yr or less (Table 1). Because ages from near the tops of ridges are only slightly younger than ages from along the weathered surface of the San Bernardino Mountains, they may represent only a slightly deeper structural level. This is consistent with local preservation of small upland surfaces in this area, such as at Chilao Flats (Fig. 2). We thus assume that the upland ridges of these blocks have experienced only several hundred meters of erosion since initiation of uplift, and thus assign erosion rates to ridge surfaces of 0.02–0.04 mm/yr. Although this is the same rate inferred for much of the weathered surface in the San Bernardino Mountains, the longer duration of this slow erosion in the San Gabriel Mountains explains the poorer preservation of low-relief surfaces. For comparison, a similar magnitude of denudation in the San Bernardino Mountains would require a faster rate of ~0.1 mm/yr, which is associated with areas of much greater relief than found on the Big Bear plateau (Fig. 7A).

Below the ridges of the Soledad and Tujunga blocks, fission track and helium ages tend to be somewhat younger, such as in Tujunga Canyon on the south and Aliso Canyon on the north (33 and 23 Ma [U-Th]/He; Table 1, Fig. 2). These ages imply average erosion rates approaching ~0.1 mm/yr. We thus infer erosion rates for canyons in these blocks by measuring the elevation difference beneath an imaginary envelope that loosely connects the ridges above. This envelope represents a paleosurface that may have once connected slowly-eroding ridges that has likely been removed across most of the western San Gabriel Mountains For example, a canyon that is ~0.4 km below the envelope would have required a rate ~0.07 mm/yr greater than along ridges to have formed by incision over the past 6 m.y., thus indicating an average erosion rate of ~0.1 mm/yr (0.07 mm/yr + 0.02–0.04 mm/yr). Exhumation rates calculated for ages in these canyons are consistent with these implied rates (Table 1; Fig. 2), although additional data in these canyons would help to test our assumptions. Estimating erosion rates in this manner essentially treats the region as a large uplifted block, in which canyons developed by vertical incision and relief increased with time.

Moving further east within the Soledad block, ridges rise in elevation and topography becomes more rugged. Despite this change, fission track and helium ages along ridges remain old (ca. 40 Ma) and imply that the imaginary structural envelope rises westward at 3–4°. Because intervening canyons remain at low elevations and do not rise to the east, relief increases eastward and our inferred erosion rates are greater than to the west (as high as 0.3–0.4 mm/yr; Fig. 7B). This pattern is broken abruptly at the San Gabriel fault, where younger fission track and helium ages are suddenly encountered to the southeast in the Pasadena block (Table 1, Fig. 2). Based on assumed closure temperature, exhumation rates in this block are ~0.2–0.3 mm/yr on ridges and ~0.4–0.5 mm/yr in canyons. Because this is roughly consistent with the block model of erosion, we infer erosion rates elsewhere in this block by differencing the elevation of canyons and an envelope connecting ridges and dividing by the duration of uplift. This pattern is locally violated near the Sierra Madre fault in the southern part of this block, where older fission track ages occur within fault slices of different thermal history (e.g., #63, Table 1, Fig. 2 and 7B) (Blythe et al., 2000).

Young ages continue eastward as the Pasadena block grades into the Sierra Madre–Baldy block (Fig. 2), with inferred erosion rates reaching as high as 1–2 mm/yr where fission track ages as low as 3 Ma are encountered in San Gabriel Canyon. This younging trend also occurs in the Soledad block. Fission track ages along ridges become young near longitude 118°, despite a general continued eastward rise in elevation. As a result, erosion rate estimates along ridges increase to 0.1–0.2 mm/yr in the Baden–Powell region, corresponding to increases in inferred erosion rates of the canyons below (Fig. 7B). It is as if the imaginary envelope represented by ca. 40 Ma ages along ridges to the west rises hundreds of meters above the topographic surface on the east. This change roughly corresponds to the point at which slopes increase significantly from west to east (Fig. 4). Although this change does not correlate with an obvious structure, it may represent a change in rock uplift associated with the deep structure of the Sierra Madre fault. Such a change could occur near Altadena, where a bend in the range front occurs and the Raymond Hill fault splays off to the southeast (Fig. 2 and 6B).

Inferred erosion rates reach a maximum in the central Baldy–Sierra Madre block, where extremely young fission track and helium ages occur along ridges and peaks. Helium ages of 5–6 Ma and fission-track ages of 7–8 Ma along high crests imply exhumation rates of 0.4 mm/yr or higher (Table 1; Fig. 7B). At lower elevations, fission-track ages as young as 3 Ma in San Gabriel Canyon imply exhumation of >1 mm/yr. Younger ages in canyons, such as a 1.8 Ma helium age below Mount San Antonio, again suggest a block model of erosion. We thus assign higher erosion rates for low regions between interfluves within this block (Fig. 7B). Although this argues that topography and erosion have not attained a steady state, in which erosion rates in ridges and valleys would be essentially equal, the regions that deviate from the 0.5–1.0 mm/yr contour interval are small in area and do not significantly impact the comparisons below. In addition, active Pleistocene-Holocene incision in San Gabriel Canyon (Bull, 1991) argues that a steady-state may not be present. Whether a steady-state model is appropriate, however, could be tested by measuring additional ages in the deepest canyons where the youngest ages should be found, such as northern San Gabriel Canyon or San Antonio Canyon.

Several small fault blocks southeast and northeast of the Baldy–Sierra Madre block have somewhat different thermal and erosional histories. The San Sevaine block south of the San Antonio fault contains older fission track ages that suggest exhumation of 0.2 mm/yr or lower. This is consistent with the occurrence of the Glendora Volcanics south of this fault and a remnant surface in the southeastern corner of the range near Cucamonga. It is slower than the Holocene rate of uplift along the Cucamonga fault (Dolan et al., 1996), however, suggesting rates have changed during the course of uplift of the range. The Blue Ridge block that occurs north of the Punchbowl–Nadeau fault contains fission track ages as young as in the Baldy block, but the inferred rapid exhumation likely does not extend northwestwards along the ridge to the Devil's Punchbowl given the presence of the late Miocene Punchbowl Formation. We thus separate a slow-erosional domain from the Blue Ridge along the intervening fault (Fig. 7B). Further north, the Table Mountain block is a narrow northwest-plunging antiform in which erosion rates as high as 0.2 mm/yr are implied by helium ages (Table 1; Fig. 2). Because exhumation has probably been greater to the southeast based on the block's structure, however, we assume erosion rates as high as 0.3 mm/yr in this block.

Although the first-order features of the estimated erosion pattern in the San Gabriel Mountains are constrained by thermochronometry, more data is needed before details can be refined. Similar to the erosion rate estimates for the San Bernardino Mountains, the pattern in Figure 7B should be viewed as a best-guess, nonunique interpretation. In addition, it is not possible to produce a reasonable estimate of uncertainty in the pattern across the San Gabriel Mountains. Due to the lack of a datum across the San Gabriel Mountains similar to the weathered surface, the pattern of erosion rates in the San Gabriel Mountains are also more poorly constrained than in the San Bernardino Mountains. To further constrain this pattern, age-elevation gradients could be measured with new samples, particularly in canyons, to test our block model of erosion.

Based on the resulting pattern, the spatially-averaged erosion rate over the past 6 m.y. in the San Gabriel Mountains is 0.35 mm/yr. This is considerably slower than the short-term rates based on sediment accumulation in debris basins along the southern, most-active perimeter of the range (Schumm, 1963; Cooke, 1984). It is also somewhat slower than estimated uplift rates along specific structures (Crook et al., 1987; Dolan et al., 1996). It is, however, greater than the spatially-averaged long-term erosion rate for the San Bernardino Mountains, although perhaps less-so than intuitively expected based on their topographic differences. The very high erosion rates in the southern San Bernardino Mountains probably make-up for the slow erosion across the Big Bear plateau, thereby resulting in comparable averages for the two ranges. However, this average erosion rate in the San Gabriel Mountains would have been present for more than twice as long as in the San Bernardino Mountains, thereby resulting in considerably greater total denudation. For example, erosion rates of 0.5–1.0 mm/yr in the Baldy Block of the San Gabriel Mountains correspond to ~6 km total denudation, whereas the same rates in the Morongo block of the San Bernardino Mountains correspond to only ~2.5 km denudation. As a result, the San Gabriel Mountains should have produced more than double the volume of sediments (average depth of erosion is 2.1 km, creating a sediment volume of 4620 km^3) for adjacent basins than the San Bernardino Mountains.

EVALUATION PATTERNS OF EROSION

Comparison of topography and erosion pattern

Although the relationship between erosion and topographic ruggedness (i.e., slope, relief) is well established (Ahnert, 1970; Schumm, 1963; Burbank et al., 1996), we compared them in the Central Transverse Ranges to see if observations were consistent. We compared mean slope, mean elevation, and average erosion rates within topographic domains. Average erosion rates for four domains in the San Gabriel Mountains and seven domains in the San Bernardino Mountains (Fig. 7) were determined by spatial analysis and plotted against the average slope and elevation calculated for the same domains using 90-m-resolution U.S. Geological Survey digital elevation models.

Results of this comparison show no clear relationship between mean elevation and slope or mean elevation and average erosion rate (Fig. 8). It is important that although we assume a block-model of erosion in the San Gabriel Mountains and the erosion pattern appears somewhat similar to topography (Figs. 2 and 7B), elevation and erosion rate are not strongly associated. However, slope and erosion rate exhibit a positive correlation (Fig. 8C). This agrees with the general rule that erosion rates and topographic slope are linked. The only domain that appears to deviate from an apparent linear increase in erosion rate with slope is the Yucaipa Ridge block of the San Bernardino Mountains. Given the likelihood that Yucaipa Ridge is at a threshold for rapid mass wasting (Spotila et al., 2001), it is unlikely that it can support steeper slopes and thus its high rock uplift rate leads to rapid erosion that forces it above the regression line. The Morongo block of the San Bernardino Mountains is the next furthest above the regression line (Fig. 8C). However, this probably results from low-slope patches within this block that can be attributed to pull-apart basins (e.g., Burro Flats) and to large landslide deposits and alluviated landslide scars (Yule and Sieh, 2002). It is interesting that the steepest domains of the San Gabriel Mountains do not exhibit erosion rates that are significantly above average for their average slope. Blythe et al. (2000) noted that the Baldy and Sierra Madre blocks exhibit average slopes that are nearly at the angle of repose for cohesionless material, similar to portions of the northwest Himalayas where high mean slopes (32°) correlate with rapid exhumation and topographic steady state (Burbank et al., 1996). If present in the eastern San Gabriel Mountains, such a steady state would invalidate our assumption of block erosion and predict that erosion rates in canyons are no greater than those on interfluves (Fig. 7B). However, the relationship of slope and erosion (Fig. 8C) does not suggest this.

This linkage between erosion rate and slope does not explain the topographic differences between the two ranges. Erosion rates may be faster on steeper slopes because of the physical behavior of individual eroding agents, but what controls the distribution of steep slopes? Put another way, steeper slopes may be maintained where erosion rates are faster, but what boundary conditions modulate erosion rate? Because of the correlation (Fig. 8C), these two questions are one in the same; what independent variables are responsible for the observed variations in the coupled slope-erosion rate system? We can address this question by comparing the spatial distribution of erosion with other parameters that may possess a causal relationship.

Comparison of active structures and erosion pattern

To the first order, the distribution and behavior of active structures are responsible for the topography and erosion patterns of the Central Transverse Ranges. Without these structures and their tectonically and geodynamically driven uplift over the past few million years (e.g., Meisling and Weldon, 1989; Humphreys and Hager, 1990; Kohler, 1999, Spotila et al., 1998; Blythe et al., 2000), these ranges would not exist. This control also persists to a finer scale, as topographic and erosion patterns within each range appear linked to structural control.

Erosion and topography of the San Bernardino Mountains are closely linked to the distribution and history of uplift structures. The Big Bear plateau has been raised along opposed, east-west trending thrust faults (Dibblee, 1975; Sadler, 1982; Spotila and Sieh, 2000). The North Frontal thrust system separates the plateau from the Mojave Desert to the north and is responsible for elevated erosion rates and rugged topography of the northern slope (Figs. 4, 6A, and 7A). The Santa Ana thrust is responsible for similar steep topography and rapid erosion along the southern plateau edge and structurally defines the low, mid-mountain Santa Ana Valley. The San Gorgonio massif similarly owes its height and form to motion along the North Frontal thrust system and associated high-angle structures that isolate it from adjacent valleys (Spotila and Sieh, 2000). The rugged topography and rapid exhumation of narrow slivers of crust trapped within the San Andreas fault are also related to structure (Spotila et al., 2001). Associations of erosion pattern and rugged topography with the distribution of major faults illustrates the important role active structures have played in the geomorphic development of the range (Figs. 4, 6A, and 7A).

Structures also play an important role in the San Gabriel Mountains. Crustal slivers within the San Andreas fault zone, including the active strand and the extinct Punchbowl–Nadeau fault, have distinct topography and independent erosion patterns that do not clearly relate to adjacent terrains (e.g., Table

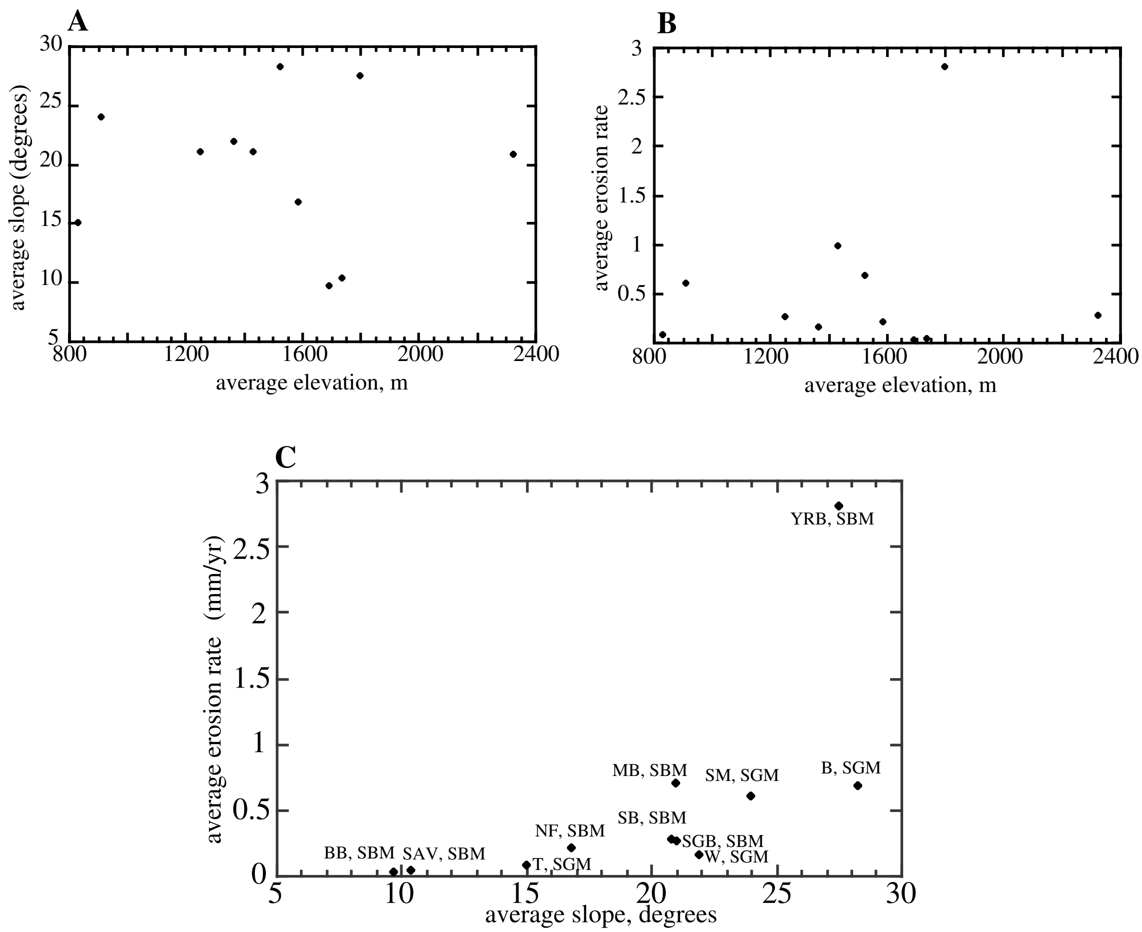

Figure 8. A: Average slope plotted against average elevation for topographic domains in both ranges. Average elevation and slope were measured using *Arc/Info* on 90 m digital elevation models for four domains in the San Gabriel Mountains (SGM) and seven domains in the San Bernardino Mountains (SBM) (areas shown on Fig. 7). B: Average erosion rate versus average elevation for the same domains. Average erosion rate for each domain was calculated as the area-weighted average assuming the median value of erosion rate for each color band in Figure 7. C: Average erosion rate versus average slope in the same domains. Individual points in the San Bernardino and San Gabriel Mountains are coded as Baldy block, BB—Big Bear plateau, MB—Morongo block, NF—northern range front domain, SAV—Santa Ana valley, SB—San Bernardino (southern) range front domain, SGB—San Gorgonio block, SM—Sierra Madre block, T—Tujunga block, W—western Soledad domain, YRB—Yucaipa Ridge block.

Mountain, Blue Ridge; Figs. 2, 6B, and 7B). Another ancient strand of the San Andreas system, the San Gabriel fault, also separates blocks that have experienced distinct thermal and erosional histories (Mahaffie, 1985; Blythe et al., 2000; Figs. 6B and 7B). Less-well known structures, including the San Antonio Canyon and Southfork Lytle Creek faults in the east, similarly influence erosion pattern (e.g., the San Sevaine block; Morton and Matti, 1993; Figs. 2, 6B, and 7B). The locus of intense erosion in the eastern portion of the range may also be related to structural features, such as the slip transfer zone between the San Jacinto and San Andreas faults or an increase in slip rate along the Sierra Madre–Cucamonga fault zone. These results are consistent with the observation that relative tectonic activity along the southern range front correlates with topographic indicators of rapid erosion (Lifton and Chase, 1992).

Although erosion patterns and topography appear to be strongly influenced by active structures, other factors may also play an influential role. There is some indication that active structures cannot explain all aspects of the erosion pattern. For example, despite the structural symmetry of the two ranges, their erosion patterns are not mirror images. The thrust faults responsible for uplift of the bulk of each range are antithetic, yet erosion in the southern San Gabriel Mountains has been more intense than in the northern San Bernardino Mountains (Fig. 7). Exhumation of blocks within the San Andreas fault zone in the southern San Bernardino Mountains has also been more intense than for blocks within the fault zone in the northern San Gabriel Mountains. These differences may stem from differences in deformation that are hidden by the simple symmetry of each range's structure, such as local convergence at the confluence of the San Andreas and San Jacinto faults in the San Gabriel Mountains or at the San Gorgonio Pass restraining bend in the San Bernardino Mountains. However, it is possible that these differences are the result of other boundary conditions. To explore this, we compare erosion pattern to bedrock, precipitation, and temporally-controlled drainage evolution below.

Comparison of bedrock erodibility and erosion patterns

Bedrock erodibility is a critical parameter for erosion and landscape evolution. Bedrock shear strength is important for resistance to frictionally driven fluvial incision (e.g., Whipple and Tucker, 1999) while fracture density, strength, and orientation are important for resistance to landsliding (e.g., Schmidt and Montgomery, 1995). As a result, bedrock variations have been shown to be important in controlling erosion in both active and extinct mountain belts (Weissel and Seidl, 1997; Hack, 1982). Lifton and Chase (1992) observed associations between short wavelength topography and lithologic variations in the San Gabriel Mountains, but did not relate larger scale topographic or erosion patterns to bedrock erodibility. Bedrock variation is thus a natural parameter to compare with estimated erosion rates both within and between the San Gabriel and San Bernardino Mountains.

To investigate the influence of bedrock erodibility on erosion, mapped bedrock lithologies must be translated into relative levels of erosional resistance. Bedrock erodibility at the scale of a hand sample may be influenced by the shear strength or hardness of individual minerals, mineralogic heterogeneity, grain size, cohesiveness of intergranular contacts, resistance to chemical breakdown, and foliation. At the outcrop scale, important parameters include heterogeneity (e.g., density of petrologic variations, such as sedimentary layering or the presence of dikes or migmatic segregation) and the degree and character of deformation (e.g., fracture density and strength, fracture orientation versus topographic slope, presence of cataclasis or pervasive shearing). Although a systematic data set representing these parameters has not been collected in the San Gabriel and San Bernardino Mountains, we infer basic differences to enable comparison.

Within each range, we have classified the basic lithologic groups (excluding Tertiary and Quaternary deposits) according to a simple scheme. Lithologic types were assigned values (1 = most susceptible to breakdown) for four parameters (Table 2). Relative mineral strength was scaled on the basis of the presence of quartz (+3), feldspar or carbonate (+2), and mica (+1). Petrologic heterogeneity was ranked as monomineralic (+2) or complex polymineralic (+1). We ranked chemical stability as stable (+2) or unstable (+1). Degree of deformation was ranked as undeformed (+2; i.e., Mesozoic plutons) or deformed (+1; Paleozoic and Precambrian rock). These values were then summed to estimate the relative resistance of each rock type. Although this classification scheme is approximate

TABLE 2. INFERRED BEDROCK ERODIBILITY IN THE CENTRAL TRANSVERSE RANGES

Lithology	Mineral strength	Petrologic heterogeneity	Chemical stability	Deformation/ metamorphic history	Total
San Bernardino Mountains					
Quartzite	3	2	2	1	8
Other granitic	2	1	2	2	7
Quartz monzonite	2	1	1	2	6
Marble	2	2	1	1	6
Baldwin gneiss	2	1	2	1	6
Gneiss, mica rich	1	1	2	1	5
San Gabriel Mountains					
Granite	2	1	2	2	7
Mt. Lowe intrusion	2	1	2	1	6
Quartz diorite	2	1	1	2	6
Gneiss	2	1	2	1	6
Anothosite	1	2	1	1	5
Gabbro	2	1	1	1	5
Mylonitic gneiss	1	1	2	1	5
Pelona Schist	1	1	1	1	4

and does not account for different erosional mechanisms at different locations (e.g., resistance to chemical denudation may be more important on the Big Bear plateau, whereas fracture density may be more important where landslides predominate), it does provide a useful qualitative description of rock erodibility.

To make the comparison, we superposed 1:250 000 scale bedrock maps (Bortugno and Spittler, 1986; Jennings and Strand, 1969) and erosion maps and computed the areal fraction of each bedrock type that corresponds with a particular interval of erosion rate. We then calculated the area-weighted average erosion rate for each bedrock type (Fig. 9). Although a monotonic relationship does not exist between inferred erodibility and average erosion rate, it is interesting that most erodible lithologies correspond to high rates of erosion, while resistant lithologies generally correspond to lower rates of erosion. Noteworthy are high erosion rate on schist and low erosion rate on quartzite. Rock type within each range may thus play a minor role in influencing erosion patterns. This association could be noncausal, however, because erodibility of distinct lithologies may be randomly associated with fault blocks of different erosional history. For example, quartz monzonite may correlate with low average erosion rate because it is the main lithology atop the Big Bear plateau, despite the fact that many outcrops of monzonite actually consist of disaggregated, erodible grus.

Given this subtle link between bedrock erodibility and erosion pattern, it is worth considering whether differences in erosion and topography between the ranges could relate to broad differences in resistance of their bedrock. This comparison is difficult, given the different petrologic and deformation histories each range has experienced. Nonetheless, there are suggestions that the San Gabriel Mountains consist of weaker bedrock than the San Bernardino Mountains. First, the San Gabriel Mountains contain several rock units that are probably very erodible or chemically unstable (e.g., mica-rich Pelona Schist or weatherable anorthosite; Bull, 1991), but lack major bodies

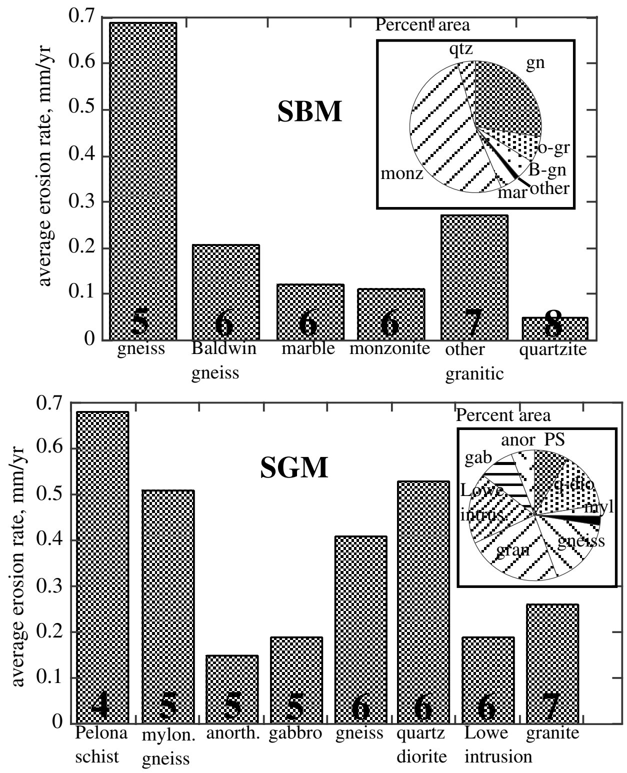

Figure 9. Bedrock versus erosion rate in the San Bernardino (SBM) and San Gabriel (SGM) Mountains. Average erosion rates are shown for the major units of the 1:250 000 scale geologic maps (Fig. 6). The average erosion rate for each rock type was measured by digitally overlaying the maps of erosion and bedrock geology, computing the average erosion rate (assuming median values of erosion rate for each color band; Fig. 7) of each bedrock body (i.e., closed polygons), and then calculating the area-weighted average of all bodies of a particular rock type. Inferred resistance to erosion is shown, with high numbers being more resistant (Table 2). Pie charts in upper right show the areal distribution of each rock type in each range. "Other granite" on the San Bernardino Mountains plot includes the Mesozoic granodiorite, diorite, and gabbro as mapped in Figure 6A. Mylonitic gneiss of the San Gabriel Mountains includes cataclastic gneiss as mapped in Figure 6B. Tertiary units and undefined metasediments were not considered. Abbreviations are: anorth/anor—anorthosite, B-gn—Baldwin gneiss, gab—gabbro, gn—gneiss, gran—granite, Lowe intrus—Mount Lowe intrusion, mar—marble, monz—monzonite, myl—mylonitic gneiss, o-gr—other granitic, PS—Pelona Schist, q-dio—quartz diorite, qtz—quartzite.

of resistant metasedimentary rock that occur in the San Bernardino Mountains (e.g., Proterozoic-Paleozoic quartzite). Thus, the San Gabriel River has exploited the weak Pelona Schist to form a rugged canyon below neighboring peaks capped by more resistant Cretaceous granodiorite (e.g., Mount Baden Powell; Ehlig, 1981; Figs. 2 and 6B), whereas quartzites in the San Bernardino Mountains form resistant ridges that armor the Big Bear plateau from encroaching streams on the north and south (e.g., Sugarloaf and Gold Mountains; Sadler and Reeder, 1983; Figs. 2 and 6A). Second, the bedrock of the San Gabriel Mountains is more heterogeneous. The number of individual bodies of crystalline rock (i.e., closed polygons defined by bedrock contacts) is greater (~170) in the San Gabriel Mountains east of Soledad Canyon than in the San Bernardino Mountains (<125) (Fig. 6), while nearly three-fourths of the bedrock in the San Bernardino Mountains consists of only two semicontinuous units (quartz monzonite and gneiss). The San Gabriel Mountains are also cut by a greater density of faults, further reducing the average size of intact rock bodies.

Another argument for greater erodibility of the San Gabriel Mountains is the greater intensity of deformation that is has experienced (Lifton and Chase, 1992; Bull, 1991). Whereas the San Bernardino Mountains lie almost entirely north of the San Andreas fault zone and are nearly autochthonous with the neighboring Mojave Desert, the San Gabriel Mountains lie within the San Andreas fault zone, consist of numerous allochthonous terranes, and have experienced penetrative deformation associated with the San Gabriel fault and the confluence of the San Jacinto and San Andreas faults (Morton, 1975; Dibblee, 1982a; Matti and Morton, 1993). Rocks at the surface of the San Gabriel Mountains have also experienced additional penetrative deformation events, such as motion along the Vincent thrust and the associated deformation of upper-plate gneiss and lower plate Pelona Schist (Ehlig, 1981; Jacobson, 1983). The least-deformed rocks of the Central Transverse Ranges are Mesozoic plutons (Ehlig, 1981; Dibblee, 1982a; Barth et al., 1995), but these make up considerably less of the San Gabriel Mountains than the San Bernardino Mountains (Fig. 6). As a result, many outcrops in the San Gabriel Mountains display extensive shearing, cataclasis, contortion, and migmatization (e.g., fractured Devil's Punchbowl basement [Dibblee, 1987], deformed Pelona Schist and overlying mylonite [Ehlig, 1981; Jacobson, 1983], closely-fractured gneiss of the San Sevaine–Cucamonga terranes [Morton, 1975; Dibblee, 1982a]), which could make them weaker than their counterparts in the San Bernardino Mountains.

Despite the likelihood that the San Gabriel Mountains basement is more erodible, the lack of quantitative constraints prevents a conclusion that this difference is the origin of differences in topography and erosion history between the ranges. Given that rocks we expect to be erodible have experienced more rapid erosion, however, a case can be made that bedrock erodibility has influenced geomorphic evolution to at least some degree.

Comparison of precipitation and erosion patterns

Precipitation pattern can exert a strong influence on erosion and topography in active mountain belts (e.g., Willett et al., 1993; Weiland and Cloos, 1996) and is thus an important parameter to compare with erosion patterns in the San Bernardino and San Gabriel Mountains. The precipitation pattern of southern California is strongly influenced by topography. Average annual precipitation in the Transverse Ranges increases rapidly from ~50 cm/yr along southern range fronts to a maximum of

~100 cm/yr along range crests, but decreases steadily northwards toward the Mojave Desert (Fig. 10A). This pattern is produced orographically by topography and the southwesterly storm track of winter storms that deliver the majority of annual precipitation (Minnich, 1986). Precipitation is forced out of rising air columns at low altitudes by the upward decrease in saturation vapor pressure associated with the adiabatic lapse rate, and thus reaches a maximum at ~2 km elevation and decreases steadily northward (Fig. 10B). This imposes a strong rain shadow on northern portions of the San Bernardino and San Gabriel Mountains and the high desert further north.

Contour diagrams of erosion rate and precipitation pattern were superposed and analyzed for the area-weighted average erosion rate within each contour band of precipitation. Erosion rate and precipitation are positively correlated in both the San Bernardino and San Gabriel Mountains (Fig. 10C). This is consistent with a positive correlation between precipitation and topographic roughness found in parts of the San Gabriel Mountains (Lifton and Chase, 1992) and suggests that precipitation patterns have significantly affected erosion in the Central Transverse Ranges. It is somewhat surprising that the correlation is so strong, however, given that complex erosion patterns are so

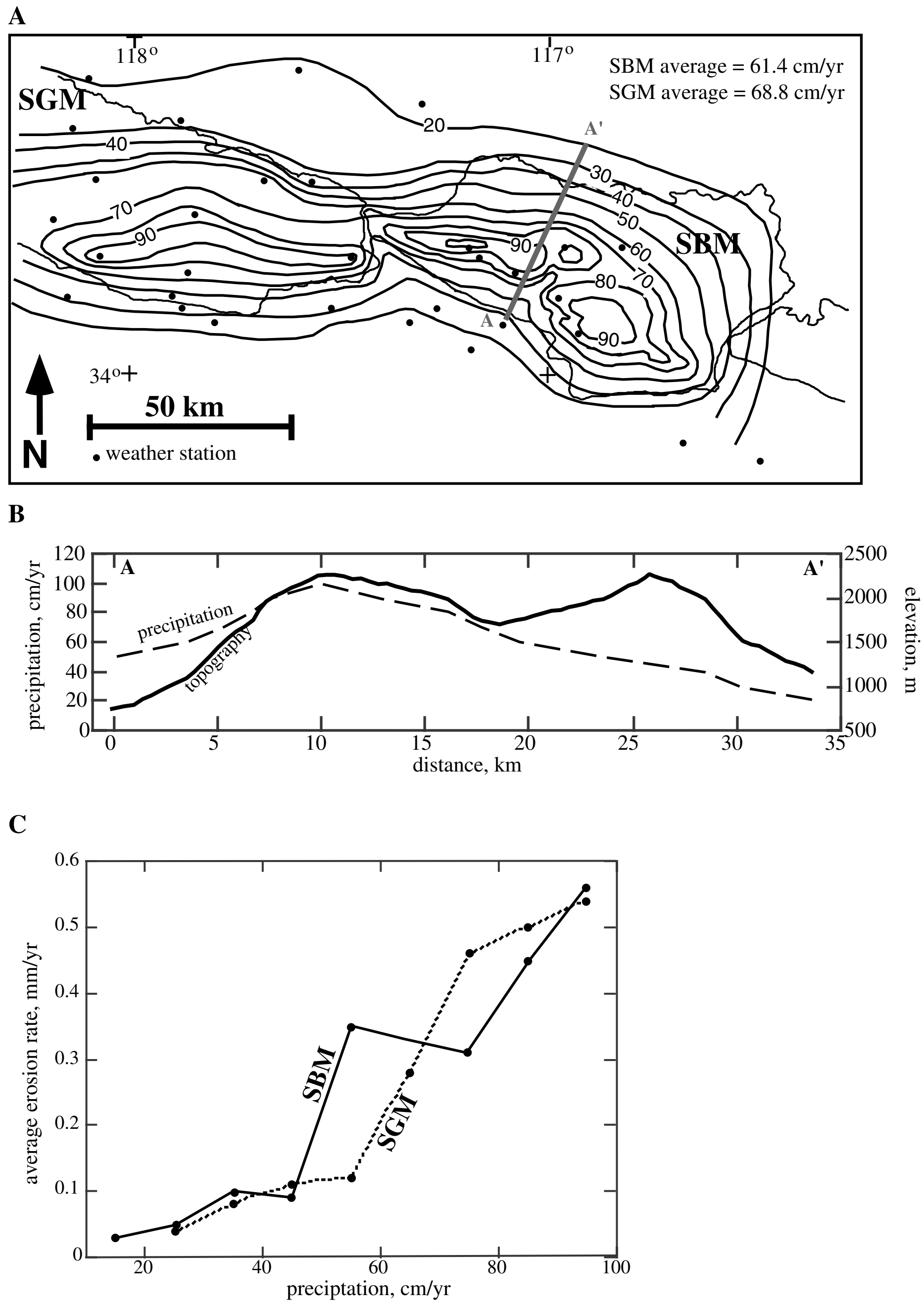

Figure 10. A: Average annual precipitation in the San Bernardino (SBM) and San Gabriel (SGM) Mountains. Contours in centimeters of total precipitation per year were hand-drawn from average annual precipitation from 1961 to 1990 at the 37 climate stations shown (data from Department of Commerce, 1993a, 1993b). Contours in the high central San Bernardino Mountains were additionally modified after the pattern shown by Minnich (1986), representing additional data and a longer time span. B: Orographically controlled precipitation along the San Bernardino Mountains. The average annual precipitation from Figure 10A (along A–A′) is plotted along an elevation profile that crosses the range in the direction of most storms (south-southwesterly winds; Minnich, 1986). C: Plot of average erosion rate and average precipitation in the two ranges. The average erosion rate for each 10 cm interval of precipitation in each range were measured by digitally overlaying the plots of erosion and precipitation and calculating the area-weighted average erosion (assuming the median value for each color band; Fig. 7) for polygons defined by each contour of mean annual precipitation.

heavily associated with the distribution of active structures. It is possible that the association between precipitation and erosion is more coincidental than causal, as the prevailing winds happen to deliver the maximum precipitation along southern range fronts where the most active structures are. At the same time, however, the activity of structures along the south may be intensified by rapid erosion accelerated by heavy precipitation (Willett, 1999).

Although it is uncertain what role precipitation plays in influencing erosion patterns, there are some complications that suggest it cannot be the main controlling agent. First, much of the precipitation that falls along the high southern crests of the San Gabriel and San Bernardino Mountains is snow, which increases long-term infiltration but does not directly increase catastrophic short-term runoff (Minnich, 1989). Second, precipitation patterns may strongly influence vegetation distribution, which in turn could affect erosion. Chaparral-covered southern hillslopes may be more resistant to erosion than northern deserts slopes dominated by sparse pinyon-juniper forest, because dense vegetation lessens the impact of rain, increases infiltration, and stabilizes hillslopes with deep root networks (Minnich, 1989). The importance of vegetation is illustrated by periodic burn events in the San Gabriel Mountains, which can lead to major increases in erosion and which further complicate the relationship of precipitation, vegetation, and erosion (cf. Bull, 1991).

A final complication is that precipitation patterns have not been static during the uplift of these ranges. As translation along the San Andreas fault modified the geography of the Central Transverse Ranges over the past few million years, orographically-controlled precipitation would have varied in response. Precipitation levels would have fluctuated as well, in association with glacial to interglacial transitions. As a result of climate change, short-lived monsoonal periods of scant vegetation cover and major tropical storms were associated with heavy hillslope erosion and valley aggradation, whereas colder, more humid periods resulted in widespread forests and more stable erosion (Bull, 1991). The duration of these fluctuations (10^3-10^4 yr) would have been much shorter than the time scale of geographic change (10^5-10^6 yr), however, such that the full range in climate variability would have been experienced by both ranges at any stage in their geomorphic evolution. Given the likelihood that the prevailing wind direction was stable during these transitions due to the geographically-controlled interaction of the jet stream and the coastal marine layer (Minnich, 1986), a pronounced rain shadow would have been probable across the San Bernardino Mountains for at least a million years while the San Gabriel Mountains blocked them from the coast. For a major portion of their short life span, the San Bernardino Mountains would have thus had significantly less precipitation than the San Gabriel Mountains. This certainly would have helped in the preservation of the deeply weathered surface across the Big Bear plateau. However, it makes the close association between long-term erosion and modern precipitation patterns (Fig. 10C) seem improbable; a comparison of time-integrated precipitation and long-term erosion would probably not have such a close correlation. This suggests that precipitation pattern is not the sole controlling agent in the patterns of erosion.

Despite these complexities, the association between erosion and precipitation cannot be ignored. Orographically-controlled precipitation has probably played an important role in the geomorphic evolution of these ranges, consistent with the view that climate patterns can strongly affect exhumation and deformation in mountain belts. The degree to which these ranges would have evolved differently had prevailing winds come from a different direction, however, remains to be explored.

Erosion pattern, time, and drainage evolution

The final variable to consider is time. Previous workers have argued that time has been the most important factor in generating geomorphic differences between these ranges, by considering their contrasting topographic "maturity" as evidence that the San Bernardino Mountains began uplifting well after the San Gabriel Mountains (e.g., Mendenhall, 1907; Vaughan, 1922; Dibblee, 1975). Although our synthesis of erosion over the duration of uplift in each range normalized the effect of time, the resulting average erosion rates are somewhat similar in each range. The longer duration of uplift in the San Gabriel Mountains thus implies greater total erosion and similarly suggests that time is an important factor in the geomorphic evolution of mountains. This is well illustrated by the drainage evolution of the San Bernardino Mountains.

One of the most remarkable aspects of topography in these ranges is the preservation of the Big Bear plateau (Fig. 4). In a traditional view, this feature would represent an immature, relict landform that has not yet been encroached upon by steepened drainages (Davis, 1899; Dibblee, 1975). The drainage network of the plateau illustrates this point, as well-integrated, meandering streams drain the plateau upland while steep, straight drainages attack the plateau margins (Mendenhall, 1907) (Fig. 5A). In one case it seems that a perimeter drainage may have broken through the divides that protect the plateau upland to capture part of the older network. This is illustrated by longitudinal profiles of Deep and Bear Creeks, tributaries to the Santa Ana River (Figs. 5A and 11). Deep Creek exhibits a concave profile that appears to have incised gradually into the westward-tilted flank of the plateau. The profile steepens to a small knickpoint at ~2000 m elevation and then becomes more gentle. It is possible that this stream follows a rough course that existed prior to uplift of the plateau and has gradually incised by means of knickpoint migration as uplift proceeded. In contrast, Bear Creek is steep and exhibits a sharp inflection where it reaches the plateau upland. Although the valley above this inflection is hidden by Big Bear Lake, the minimal elevation difference from Big Bear Dam to the lake's eastern shore in-

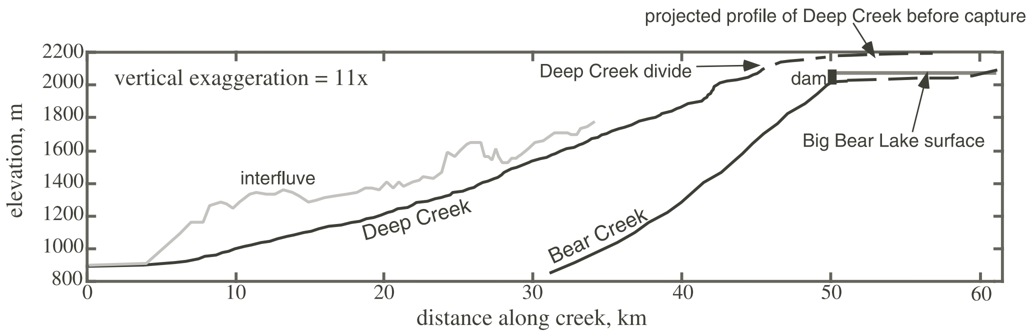

Figure 11. Longitudinal profiles along Deep Creek and Bear Creek in the San Bernardino Mountains. Compare to Figure 2 and 5A for locations. Profile begins in the northwest where Deep Creek joins the Mojave River. The interfluve above Deep Creek is shown, to illustrate the gentle tilt of the western flank of the plateau. Bear Creek starts on the south where the Santa Ana River leaves the range front. It continues north to Big Bear dam. Although the artificial Big Bear Lake covers the valley, Big Bear Valley once drained into Bear Creek. This former valley bottom is of gentle grade, based on the elevation of the base of the dam and the eastern shore of the lake. The interpolated valley bottom is similar in slope and elevation (although ~100 m lower) than the eastward project of Deep Creek across the canyon now formed by Bear Creek. This profile and the adjacent location of the upper reaches of these streams argue for drainage capture of a portion of the Deep Creek basin by the Bear Creek–Santa Ana River.

dicates that a gentle trunk was flooded by this artificial lake (Fig. 11). The similar elevation and geographic alignment of this trunk stream with the upper reach of Deep Creek suggests that Bear Creek broke through the plateau's southern divide and captured a portion of a relict drainage network (Sadler and Reeder, 1983) (Figs. 5A and 11). The slightly lower elevation of the base of Bear Valley implies that this capture resulted in more rapid erosion upstream of Bear Creek than along the beheaded headwaters of Deep Creek. That this represents the only major break in the plateau's east-west divides and that the intervening canyon is the steepest part of the plateau supports this hypothesis (Figs. 2 and 7A).

This case of drainage capture suggests that the present topography of the San Bernardino Mountains is a window into a transitional stage of geomorphic evolution. As more time passes, the Big Bear plateau may become more similar in appearance to the San Gabriel Mountains. It is also possible that as this happens, erosion rates in the San Bernardino Mountains may increase. A positive feedback may exist, in which increased incision leads to more rugged slopes, which in turn leads to more rapid erosion. With time, the difference in long-term erosion rate between the two ranges could thus become smaller. This represents a plausible anecdote that explains the differences in topography and erosion pattern as a result of different uplift duration between the ranges.

Based on the comparisons with other parameters above, however, there are ample reasons other than uplift duration why the San Bernardino Mountains should be less eroded. For example, the erosional resistance of the homogenous Mesozoic batholith and metasedimentary roof pendants of the San Bernardino Mountains may have made the headward erosion of steep marginal streams slower than in the San Gabriel Mountains (Figs. 5, 6, and 7). The opposed nature of the two thrust faults in the San Bernardino Mountains may have also resulted in asymmetric divides on the north and south, which when armored with resistant lithologies may have protected the upland from erosion. The San Gabriel Mountains lack these divides and have only small, isolated bodies of resistant rock that are not aligned with range fronts. At the same time, the San Gabriel Mountains have probably received a greater magnitude of precipitation over the past few million years. This suggests that the San Gabriel Mountains may have passed more rapidly through geomorphic stages, so that even if duration had been equal, they would be more eroded than the San Bernardino Mountains.

Unfortunately, there is no means at present to evaluate the relative role of uplift duration and other parameters in the geomorphic evolution of these ranges. As erosion continues over time, old surfaces, inherited drainages, and the plateau itself will certainly be removed from the San Bernardino Mountains. Once removed, erosion rates may actually increase as drainages become graded and more efficient at competing with rock uplift. However, it is not clear whether this evolution will require more time than it did in the San Gabriel Mountains, because of their different boundary conditions.

CONCLUSIONS

We have compared several parameters to erosion rates in the San Gabriel and San Bernardino Mountains, to determine the origin of their different topographic expressions and to better understand what controls the geomorphic evolution of active mountain belts. These comparisons are enabled by estimates of long-term erosion constructed from thermochronometric and geologic data. Although these estimates are nonunique and in many respects speculative, they do offer insight into the geomorphic evolution of active orogens.

In both ranges, erosion rate and topographic slope appear coupled, such that independent controls on topography and independent controls on erosion are one in the same. Therefore, the observed correlation does not help explain differences in geomorphology and erosion within and between the ranges. Within each range, long-term erosion rates also associated with the distribution of active deformation, inferred bedrock erodibility, and mean annual precipitation. Any or all of these parameters may be key to the erosion and topographic evolution of each range. The differences in erosion and geomorphic expression between these two ranges may similarly be explained by differences in active structures, lithology, and precipitation pattern over the past few million years. However, it is just as likely that the difference in the duration of uplift between these ranges is responsible for their differences.

Because all of the parameters considered important for erosion and topographic evolution of mountains are associated with erosion rates in the San Gabriel and San Bernardino Mountains, it is not possible to extract the relative importance of each parameter or to determine whether all associations are causal. It is possible that many associations are simply due to spatial coincidence of variables in the rapidly or slowly-eroding portions of each range. Given that each parameter can be linked theoretically or empirically with erosional processes, however, it is not surprising that each bears a relationship to erosion in these ranges. It is likely that to some degree, each parameter plays a deterministic role in the erosion and geomorphic evolution of the Transverse Ranges. The best way to describe the geomorphic evolution of these ranges may simply be that rapid erosion occurs where numerous parameters favoring rapid erosion are coincident, whereas slower erosion occurs where parameters that hinder erosion are coincident, and in either case these effects are magnified over time. Such an explanation can be considered a coincident determinism, in which common occurrence of independent, influential variables controls geomorphic expression and erosion of mountains. To further explore these controls on erosion, they must be compared in studies of geomorphically-distinct mountains that are more similar with respect to boundary conditions. Numerical simulations of erosion and topographic evolution in the San Gabriel and San Bernardino Mountains may also be a useful future direction of study.

ACKNOWLEDGMENTS

We thank Peter Sadler, Andrew Barth, and an anonymous reviewer for helpful reviews of this manuscript and general help in understanding the Transverse Ranges. Gratitude is also extended to the following, who helped at various times with data interpretation and general understanding: K. Farley, K. Sieh, D. Yule, L.T. Silver, R.P. Sharp, and M. Mahaffie.

REFERENCES CITED

Ahnert, F., 1970, A comparison of theoretical slope models with slopes in the field: Zeitschrift fur Geomorphologie Supplement Bd., v. 9, p. 88–101.

Albright, B., 1999, Magnetostratigraphy and biochronology of the San Timoteo Badlands, southern California, with implications for local Pliocene-Pleistocene tectonic and depositional patterns: Geological Society of America Bulletin, v. 111, p. 1265–1293.

Allen, C.R., 1957, San Andreas fault zone in San Gorgonio Pass, southern California, Geological Society of America Bulletin, v. 68, p. 315–350.

Andrews, J.T., 1972, Glacier power, mass balances, velocities, and erosion potential: Zeitschrift fur Geomorphologie N.F., Supplement Bd., v. 13, p. 1–17.

Atwater, T., 1970, Implications of plate tectonics for the Cenozoic tectonic evolution of western North America, Geological Society of America Bulletin, v. 81, p. 3513–3536.

Axelrod, D.I., 1950, Evolution of desert vegetation in western North America, *in* Studies in late Tertiary Paleobotany: Carnegie Institute Washington Publication, v. 590, p. 215–306.

Baird, A.K., Morton, D.M., Woodford, A.O., and Baird, K.W., 1974, Transverse Ranges Province: A unique structural-petrochemical belt across the San Andreas fault system: Geological Society of America Bulletin, v. 85, p. 163–174.

Baldwin, J.A., Whipple, K.X., and Tucker, G.E., 2002, Implications of the shear-stress river incision model for the timescale of postorogenic decay of topography: Journal of Geophysical Research (in press).

Barth, A.P., Wooden, J.L., Tosdal, R.M., and Morrison, J., 1995, Crustal contamination in the petrogenesis of a calc-alkaline rock series: Josephine Mountain intrusion, California: Geological Society of America Bulletin, v. 107, p. 201–212.

Beaumont, C., Fullsack, P., and Hamilton, J., 1992, Erosional control of active compressional systems, *in* McClay, K.R., ed., Thrust tectonics: New York, Chapman Hall, p. 1–18.

Bierman, P., and Turner, J., 1995, ^{10}Be and ^{26}Al evidence for exceptionally low rates of Australian bedrock erosion and the likely existence of pre-Pleistocene landscapes: Quaternary Research, v. 44, p. 378–382.

Blythe, A.E., Burbank, D.W., Farley, K.A., and Fielding, E.J., 2000, Structural and topographic evolution of the central Transverse Ranges, California, from apatite fission-track (U-Th)/He and digital elevation model analyses: Basin Research, v. 12, p. 97–114.

Bortugno, E.J., and Spittler, T.E., 1986, Geologic map of the San Bernardino quadrangle, California, 1:250 000, California Division of Mines and Geology: Regional Geologic Map Series, Map No. 3A.

Brown, G., et al., 1976, Geology and ground water geology of Big Bear Valley: Association of Engineering Geologists, So. California Section, Annual Spring Field Trip Guidebook, p. 73–95.

Bull, W.B., 1991, Geomorphic Responses to Climate Change: London, Oxford University Press, 326 p.

Burbank, D.W., Leland, J., Fielding, E., Anderson, R.S., Brozovic, N., Reid, M., and Duncan, C., 1996, Bedrock incision, rock uplift and threshold hillslopes in the northwestern Himalayas: Nature, v. 379, p. 505–510.

Cooke, R.U., 1984, Geomorphological Hazards in Los Angeles: London, George Allen and Unwin, 206 p.

Crook, R., Jr., Allen, C.R., Kamb, B., Payne, C.M., and Proctor, R.J., 1987, Quaternary geology and seismic hazard of the Sierra Madre and associated faults, western San Gabriel Mountains, *in* Morton, D.M., and Yerkes, R.F., eds., Recent reverse faulting in the Transverse Ranges, California: U.S. Geological Survey Professional Paper 1339, p. 27–63.

Crowell, J.C., 1982, The tectonics of the Ridge Basin, southern California, *in* Crowell, J.C., and Link, M.H., eds., Geologic history of the Ridge Basin, southern California, Pacific Section: Society of Economic Paleontologists and Mineralogists, p. 25–42.

Davis, W.M., 1899, The geographical cycle: Geographical Journal, v. 14, p. 481–504.

DeMets, C., 1995, Reappraisal of seafloor spreading lineations in the Gulf of California: Implications for the transfer of Baja California to the Pacific Plate and estimates of Pacific-North America motion: Geophysical Research Letter, v. 22, p. 3545–3548.

Densmore, A.L., Anderson, R.L., McAdoo, B.G., and Ellis, M.A., 1997, Hillslope evolution by bedrock landslides: Science, v. 275, p. 369–372.

Department of Commerce, 1993a, Climatological data annual summary: California, 97: 13, NOAA, Department of Commerce.

Department of Commerce, 1993b, Hourly precipitation data: California, v. 38–43, NOAA, National Climatic Data Center, National Environmental Data and Information Service, Department of Commerce.

Dibblee, T.W., 1975, Late Quaternary uplift of the San Bernardino Mountains on the San Andreas and related faults, *in* Crowell, J.C., ed., San Andreas fault in southern California: California Division of Mines Geology Special Report, 118, p. 127–135.

Dibblee, T.W., 1982a, Geology of the San Gabriel Mountains, southern California, *in* Fife, D.L., and Minch, J.A., eds., Geology and Mineral Wealth of the California Transverse Ranges: Santa Ana, California, South Coast Geological Society, p. 131–147.

Dibblee, T.W., 1982b, Geology of the San Bernardino Mountains, southern California, *in* Fife, D.L., and Minch, J.A., eds., Geology and Mineral Wealth of the California Transverse Ranges: Santa Ana, California, South Coast Geological Society, p. 148–169.

Dibblee, T.W., 1987, Geology of the Devil's Punchbowl, Los Angeles County, California: Geological Society of America Centennial Field Guide, Cordilleran Section, p. 207–210.

Dickinson, W.R., 1996, Kinematics of transrotational tectonism in the California Transverse Ranges and its contribution to cumulative slip along the San Andreas transform fault system: Boulder, Colorado, Geological Society of America Special Paper 305, 46 p.

Dillon, J.T., and Ehlig, P.L., 1993, Displacement on the southern San Andreas fault, *in* Powell, R.E., et al., eds., The San Andreas fault system: Displacement, palinspastic reconstruction, and geologic evolution: Boulder, Colorado, Geological Society of America Memoir 178, p. 199–216.

Dolan, J.F., Jordon, F., Rasmussen, G., Stevens, D., Reeder, W., and McFadden, L.M., 1996, Evidence for probable moderate-sized (Mw 6.5–7.0) paleoearthquake on the Cucamonga fault, northwestern Los Angeles metropolitan region, California: (abstract), Eos (Transactions, American Geophysical Union), v. 77, Fall Meeting Supplement F461.

Eden, M.J., 1971, Some aspects of weathering and landform formation in Guyana (formerly British Guiana): Zeitschrift fur Geomorphologie, v. 15, p. 181–198.

Edmond, J.M., Palmer, M.R., Measures, C.I., Grant, B., and Stallard, R.F., 1995, The fluvial geochemistry and denudation rate of the Guayana Shield in Venezuela, Columbia, and Brazil: Geochimica et Cosmochimica Acta, v. 59, p. 3301–3325.

Ehlert, K.W., 1989, Postmiddle Miocene offset of the mint Canyon and Caliente Formations along the San Andreas and San Gabriel faults: South Coast Geological Society, p. 151–167.

Ehlig, P.L., 1981, Original and tectonic history of the basement terrane of the San Gabriel Mountains, central Transverse Ranges, *in* Ernst, W.G., ed., The geotectonic development of California (Rubey Volume I): Englewood Cliffs, New Jersey, Prentice Hall, p. 254–283.

Farley, K.A., 2000, Helium diffusion from apatite: General behavior as illustrated by Durango fluorapatite: Journal of Geophysical Research, v. 105, p. 2903–2914.

Hack, J.T., 1960, Interpretation of erosional topography in humid temperate regions: American Journal of Science, v. 258-A, p. 80–97.

Hack, J.T., 1982, Physiographic divisions and differential uplift in the Piedmont and Blue Ridge: U.S. Geological Survey Professional Paper 1265, 49 p.

Hancock, G.D., Anderson, R.S., and Whipple, K.X., 1999, Beyond Power: Bedrock incision process and form, *in* Tinkler, K.J., and Wohl, E.E., eds., Rivers Over Rock: Fluvial Processes in Bedrock Channel: Washington, D.C., American Geophysical Union, p. 35–60.

House, M.A., and Blythe, A.E., 2000, Evidence for spatially complex late Cenozoic uplift and exhumation of the eastern San Gabriel Mountains from (U-Th)/He thermochronometry [abstract]: Southern California Earthquake Center Annual Meeting, Oxnard, California, September, 2000.

Hovius, N., Stark, C., and Allen, P., 1997, Sediment flux from a mountain belt derived by landslide mapping: Geology, v. 25, p. 231–234.

Humphreys, E.D., and Hager, B.H., 1990, A kinematic model for the late Cenozoic development of southern California crust and upper mantle: Journal of Geophysical Research, v. 95, p. 19 747–19 762.

Ingersoll, R.V., and Rumelhart, P.E., 1999, Three stage evolution of the Los Angeles basin, southern California: Geology, v. 27, p. 593–596.

Jacobs, S.E., 1982, Geology of a part of the upper Santa Ana River Valley, San Bernardino Mountains, San Bernardino County, California [M.S. thesis]: Los Angeles, California, California State University, 107 p.

Jacobson, C.E., 1983, Structural geology of the Pelona Schist and Vincent thrust, San Gabriel Mountains, California: Geological Society of America Bulletin, v. 94, p. 753–767.

Jennings, C.W., and Strand, R.G., 1969, Geologic map of California, Los Angeles sheet: California Division of Mines and Geology.

Kohler, M.D., 1999, Lithospheric deformation beneath the San Gabriel Mountains in the southern California Transverse Ranges: Journal of Geophysical Research, v. 104, p. 15 025–15 041.

Koons, P., 1995, Modeling the topographic evolution of collisional belts: Annual Rev. Earth Planetary Sciences, v. 23, p. 375–408.

Lifton, N.A., and Chase, C.G., 1992, Tectonic, climatic and lithologic influences on landscape fractal dimension and hypsometry: Implications for landscape evolution in the San Gabriel Mountains, California: Geomorphology, v. 5, p. 77–114.

Mabbutt, J.A., 1965, The weathered land surface in Central Australia: Zeitschrift fur Geomorphologie, v. 9:1, p. 82–114.

Mahaffie, M.J., 1985, Implications of fission-track thermochronology for the tectonic evolution of the eastern San Gabriel Mountains, California [M.S. thesis]: Louisiana State University, 49 p.

Mancktelow, N., and Grasemann, B., 1997, Time-dependent effects of heat advection and topography on cooling histories during erosion: Tectonophysics, v. 270, p. 167–195.

Masek, J.G., Isacks, B.L., Gubbels, T.L., and Fielding, E.J., 1994, Erosion and tectonics at the margins of continental plateaus: Journal of Geophysical Research, v. 99, p. 13 941–13 956.

Matti, J.C., and Morton, D.M., 1993, Paleogeographic evolution of the San Andreas fault in southern California: A reconstruction based on a new cross-fault correlation, *in* Powell, R.E., et al., eds., The San Andreas fault system: Displacement, palinspastic reconstruction, and geologic evolution: Boulder, Colorado, Geological Society of America Memoir 178, p. 107–159.

May, S.R., and Repenning, C.A., 1982, New evidence for the age of the Old Woman sandstone, Mojave Desert, California, *in* Cooper, J.D., ed., Geologic excursions in the Transverse Ranges: Anaheim, California, Geological Society of America Cordilleran Section Meeting Guidebook, v. 78, p. 93–96.

Meisling, K.E., and Weldon, R.J., 1989, Late Cenozoic tectonics of the northwestern San Bernardino Mountains, southern California: Geological Society of America Bulletin, v. 101, p. 106–128.

Mendenhall, W.C., 1907, Two mountain ranges in southern California (abstract): Geological Society of America Bulletin, v. 18, p. 660–661.

Minnich, R.A., 1986, Snow levels and amounts in the mountains of southern California: Journal of Hydrology, v. 89, p. 37–58.

Minnich, R.A., 1989, Climate, fire and landslides in southern California, *in* Sadler, P.M., and Morton, D.M., eds., Landslides in a Semi-Arid Environment: Publications of the Inland Geological Society, v. 2, p. 91–100.

Morton, D.M., 1975, Synopsis of the geology in the eastern San Gabriel Mountains, southern California, *in* Crowell, J.C., ed., San Andreas fault in southern California: California Division of Mines Geology Special Report 118, p. 170–176.

Morton, D.M., and Matti, J.C., 1993, Extension and contraction within an evolving divergent strike-slip fault complex: The San Andreas and San Jacinto fault zones at their convergence in southern California, *in* Powell, R.E., et al., eds., The San Andreas fault system: Displacement, palinspastic reconstruction, and geologic evolution: Boulder, Colorado, Geological Society of America Memoir 178, p. 217–230.

Nagy, E.A., and Stock, J.M., 2000, Structural controls on the continent-ocean transition in the northern Gulf of California: Journal of Geophysical Research, v. 105, p. 16 251–16 270.

Neville, S.L., and Chambers, J.M., 1982, Late Miocene alkaline volcanism, northeastern San Bernardino Mountains and adjacent Mojave Desert, *in* Cooper, J.D., ed., Geologic excursions in the Transverse Ranges: Fullerton, California, Geological Society of America Annual Meeting Guidebook, California State University, p. 103–106.

Oberlander, T.M., 1972, Morphogenesis of granitic boulder slopes in the Mojave Desert, California: Journal of Geology, v. 80, p. 1–20.

Ollier, C.D., 1975, Weathering: London, Longman Group Limited, 304 p.

Paterson, W.S.B., 1994, The Physics of Glaciers: Oxford, UK, Elsevier, 480 p.

Pavich, M.J., 1986, Processes and rates of saprolite production and erosion on a foliated granitic rock of the Virginia Piedmont, *in* Colman, S.M., and Dethier, D.P., eds., Rates of Chemical Weathering of Rocks and Minerals: Academic Press Inc., p. 552–590.

Pinet, P, and Souriau, M., 1988, Continental erosion and large-scale relief: Tectonics, v. 7, p. 563–582.

Powell, R.E., 1982, Prebatholithic terranes in the crystalline basement complex of the Transverse Ranges, southern California: Geological Society of America Abstracts with Programs, v. 14, no. 4, 225 p.

Powell, R.E., 1993, Balanced palinspastic reconstruction of prelate Cenozoic paleogeology, southern California: Geologic and kinematic constraints on evolution of the San Andreas fault system, *in* Powell, R.E., et al., eds., The San Andreas fault system: Displacement, palinspastic reconstruction, and geologic evolution: Boulder, Colorado, Geological Society of America Memoir 178, p. 1–106.

Power, E.T., and Smith, B.J., 1994, A comparative study of deep weathering and weathering products: Case studies from Ireland, Corsica, and Southeast Brazil, *in* Robinson, D.A., and Williams, R.B.G., eds., Rock Weathering and Landform Evolution: John Wiley and Sons, p. 21–40.

Proctor, R.J., 1968, Geology of the upper Coachella Valley area, California: California Division of Mines and Geology Special Report 94, p. 8–43.

Reynolds, R.E., and Reeder, W.A., 1986, Age and fossil assemblages of the San Timoteo Formation, Riverside County, California, *in* Kooser, M.A., and Reynolds, R.E., eds., Geology Around the Margins of the Eastern San Bernardino Mountains: Redlands, California, Pub. Inland Geological Society, Inland Geological Society, v. 1, p. 51–56.

Rumelhart, P.E., and Ingersoll, R.V., 1997, Provenance of the upper Miocene Modelo Formation and subsidence analysis of the Los Angeles basin, southern California: Implications for paleotectonic and paleogeographic reconstructions: Geological Society of America Bulletin, v. 109, p. 885–899.

Ruxton, B.P., and Berry, L., 1957, Weathering of granite and associated erosional features in Hong Kong: Geological Society of America Bulletin, v. 68, p. 1263–1292.

Sadler, P.M., 1982, Provenance and structure of late Cenozoic sediments in the northeast San Bernardino Mountains, *in* Cooper, J.D., ed., Geologic excursions in the Transverse Ranges: Anaheim, California, Geological Society of America Cordilleran Section Meeting Guidebook 78, p. 83–91.

Sadler, P.M., 1993, The Santa Ana basin of the central San Bernardino Mountains: Evidence of the timing and uplift and strike-slip relative to the San Gabriel Mountains, *in* Powell, R.E., et al., eds., The San Andreas fault system: Displacement, palinspastic reconstruction, and geologic evolution: Boulder, Colorado, Geological Society of America Memoir 178, p. 307–322.

Sadler, P.M., and Reeder, W.A., 1983, Upper Cenozoic, quartzite-bearing gravels of the San Bernardino Mountains, southern California: Recycling and mixing as a result of transpressional uplift, *in* Anderson, D.W., and Rymer, M.J., eds., Tectonics and sedimentation along faults of the San Andreas system: Los Angeles, California, Society of Economic Paleontologists and Mineralogists, Pacific Section, p. 45–57.

Sadler, P.M., Demirer, A., West, D., and Hillenbrand, J.M., 1993, The Mill Creek basin, the Potato sandstone, and fault strands in the San Andreas fault south of the San Bernardino Mountains, *in* Powell, R.E., et al., eds., The San Andreas fault system: Displacement, palinspastic reconstruction, and geologic evolution: Boulder, Colorado, Geological Society of America Memoir 178, p. 289–306.

Saunders, I., and Young, A., 1983, Rates of surface processes on slopes, slope retreat, and denudation: Earth Surface Processes and Landforms, p. 473–501.

Schmidt, K., and Montgomery, D., 1995, Limits to relief: Science, v. 270, p. 617–620.

Schumm, S., 1963, Disparity between present rates of denudation and orogeny: U.S. Geological Survey Professional Paper 454-H, 13 p.

Spotila, J.A., 1999, The neotectonics of the San Bernardino Mountains and adjacent San Andreas fault: A case study of uplift associated with strike-slip fault systems [Ph.D. thesis]: Pasadena, California, California Institute of Technology, 378 p.

Spotila, J.A., and Sieh, K., 2000, Architecture of transpressional thrust faulting in the San Bernardino Mountains, southern California, from deformation of a deeply weathered surface: Tectonics, v. 19, p. 589–615.

Spotila, J.A., Farley, K.A., and Sieh, K., 1998, Uplift and erosion of the San Bernardino Mountains associated with transpression along the San Andreas fault, California, as constrained by radiogenic helium thermochronometry: Tectonics, v. 17, p. 360–378.

Spotila, J.A., Farley, K.A., Yule, J.D., and Reiners, P.W., 2001, Near-field transpressive deformation along the San Andreas fault zone in southern California, based on exhumation constrained by (U-Th)/He dating: Journal of Geophysical Research, v. 106, p. 30 909–30 922.

Strahler, A.N., 1952, Hypsometric (area-altitude) analysis of erosional topography: Geological Society of America Bulletin, v. 63, p. 1117–1142.

Sylvester, A.G., 1988, Strike-slip faults: Geological Society of America Bulletin, v. 100, p. 1666–1703.

Teeuw, R.M., Thomas, M.F., and Thorp, M.B., 1994, Regolith and landscape development in the Koidu Basin of Sierra Leone, *in* Robinson, D.A., and Williams, R.B.G., eds., Rock Weathering and Landform Evolution, John Wiley and Sons, p. 303–320.

Tippet, J.M., and Kamp, P.J., 1995, Quantitative relationships between uplift and relief parameters for the Southern Alps, New Zealand, as determined by fission track analysis: Earth Surface Processes and Landforms, v. 20, p. 153–175.

Treiman, J., 1982, Age of upper Saugus Formation at Newhall, California, and implications as to the age of the Santa Susana Mountains, *in* Fife, D.L., and Minch, J.A., eds., Geology and mineral wealth of the California Transverse Ranges: Santa Ana, California, South Coast Geological Society, p. 330.

Vauchez, A., and Nicolas, A., 1991, Mountain building: Strike-parallel motion and mantle anisotropy: Tectonophysics, v. 185, p. 183–201.

Vaughan, F.W., 1922, Geology of the San Bernardino Mountains north of San Gorgonio Pass: University of California Publication in Geological Sciences, v. 13, p. 319–411.

Weigand, P.W., 1982, Middle Cenozoic volcanism of the western Transverse Ranges, *in* Fife, D.L., and Minch, J.A., eds., Geology and Mineral Wealth of the California Transverse Ranges: Santa Ana, California, South Coast Geological Society, p. 170–188.

Weiland, R., and Cloos, M., 1996, Pliocene-Pleistocene asymmetric unroofing of the Irian fold belt, Irian Jaya, Indonesia: Apatite fission track thermochronlogy: Geological Society of America Bulletin, v. 108, p. 1438–1449.

Weissel, J.K., and Seidl, M.A., 1997, Influence of rock strength properties on escarpment retreat across passive continental margins: Geology, v. 25, p. 631–634.

Weldon, R.J., Meisling, K.E., and Alexander, J., 1993, A speculative history of the San Andreas fault in the central Transverse Ranges, California, *in*

Powell, R.E., et al., eds., The San Andreas fault system: Displacement, palinspastic reconstruction, and geologic evolution: Boulder, Colorado, Geological Society of America Memorial 178, p. 161–198.

Whipple, K., and Tucker, G., 1999, Dynamics of bedrock channels in active orogens: Implications for height limits of mountain ranges, landscape response timescales, and research needs: Journal of Geophysical Research, v. 104, p. 17 661–17 674.

Willett, S., Beaumont, C., and Fullsack, P., 1993, Mechanical models for the tectonics of doubly vergent compressional orogens: Geology, v. 21, p. 371–374.

Willett, S.D., 1999, Orogeny and orography: The effects of erosion on the structure of mountain belts: Journal of Geophysical Research, v. 104, p. 28 957–28 981.

Williams, A.G., Ternan, L., and Kent, M., 1986, Some observations on the chemical weathering of the Dartmoor granite: Earth Surface Processes and Landforms, v. 11, p. 557–574.

Wolf, R.A., Farley, K.A., and Silver, L.T., 1996, Helium diffusion and low temperature thermochronometry of apatite: Geochimica et Cosmochimica Acta, v. 60, p. 4231–4240.

Woodburne, M.O., 1975, Cenozoic stratigraphy of the Transverse Ranges and adjacent areas, southern California: Boulder, Colorado, Geological Society of America Special Paper 162, 91 p.

Wright, T.L., 1991, Structural geology and tectonic evolution of the Los Angeles basin, California, *in* Biddle, K.T., ed., Active margin basins: American Association of Petroleum Geologists Memoir 52, p. 35–134.

Yule, J.D., and Sieh, K., 2002, Complexities of the San Andreas fault near San Gorgonio Pass: Implications for large earthquakes: Journal of Geophysical Research (in press).

Manuscript Accepted by the Society February 8, 2002

Printed in the U.S.A.